J. Fluid Mech. (1991), *vol.* 233, *pp.* 405–437
Printed in Great Britain

The axisymmetric thermocapillary motion of a fluid particle in a tube

By JINNAN CHEN[1], ZEEV DAGAN[1] AND CHARLES MALDARELLI[2]†

[1] Department of Mechanical Engineering, City College of New York, NY 10031, USA

[2] Levich Institute for Physicochemical Hydrodynamics, Department of Chemical Engineering, City College of New York, NY 10031, USA

(Received 8 January 1991 and in revised form 28 May 1991)

The thermocapillary migration of a fluid particle in a tube, owing to an imposed axial temperature gradient, is studied theoretically for the case of steady, axisymmetric, creeping, translation in the absence of thermal convection and fluid particle distortion from sphericity, and for an insulated tube. Formulated with these assumptions, the migration is a linear Stokes flow which is separable into two fixed-fluid particle flow idealizations. One is the fluid motion in a quiescent continuous phase, owing only to the thermocapillary surface stress. This stress causes fluid streaming which exerts a lift force on the fluid particle in the direction of the warmer fluid described by a lift coefficient. The second idealization is uniform flow in the absence of thermocapillary forces. The force on the fluid particle owing to this flow represents the hydrodynamic resistance to the forward motion of the fluid particle in the presence of the tube wall, and is described in terms of a drag coefficient. Numerical solutions for the lift and drag coefficients are obtained by a boundary collocation technique.

The migration velocity in the tube relative to that under identical conditions in an infinite medium is computed from the ratio of the lift and drag coefficients. The calculations show that for a fixed ratio of the sphere to the tube diameter, as the conductivity of the fluid particle phase decreases relative to that of the continuous phase, a greater proportion of energy is conducted through the gap between the insulated tube wall and the fluid particle. This conduction pattern creates a larger surface temperature gradient, and causes the relative migration velocity to increase. The enhancement in migration for decreasing fluid particle conductivity at a fixed ratio of the sphere to the tube diameter becomes more pronounced as the later ratio increases and the surface gradient intensifies. However, as the gap distance between the sphere and the tube decreases, hydrodynamic retarding forces develop, and these forces are overriding in the sense that the relative migration velocity in the tube decreases monotonically from the value of one as the gap thickness decreases, and therefore the migration velocity in the tube never exceeds the value in an infinite medium.

1. Introduction

Gas bubbles or liquid droplets situated in a thermally stratified continuous liquid phase migrate in the direction of increasing temperature. The physicochemical basis

† To whom correspondence should be addressed.

for this migration is the decreasing dependence of the interfacial tension of the fluid interface of the bubble or drop on the temperature. As the fluid particle contacts the imposed thermal gradient of the continuous phase, one end of its surface becomes warmer than the opposite end. The surface tension at the warmer end is reduced relative to that at the cooler end, and an interfacial tension gradient or Marangoni force is created which tugs the interface in the direction of the cooler pole. This action creates in the exterior phase an opposing tangential viscous shear traction as it forces a streaming of the continuous phase liquid immediately adjacent to the interface in the direction of the cooler end of the fluid particle. The fluid streaming causes a higher pressure to develop just beyond the cooler end (relative to the pressure at the warmer end) which opposes the flow and preserves an undisturbed state at extended regions away from the fluid particle. The actions of the opposing tangential shear and the higher pressure at the cooler end provide a lift force which drives the fluid particle through the continuous liquid in the direction of the higher temperature. At steady state, the lift force is balanced by the pressure and viscous shear forces acting on the fluid particle which retard the forward motion.

A theoretical study of the thermocapillary migration of a single gas bubble in an unbounded continuous phase was first undertaken by Young, Goldstein & Block (1959), neglecting fluid inertia (low Reynolds number, Re) and the convective transport of energy (low Péclet number, Pe). In these limits the spherical shape is an exact solution of the governing equations, and thus no restriction on the capillary number (Ca), the ratio of the magnitudes of distending tractions to the surface tension force, need be imposed. This fundamental solution has been corrected to examine the influences of finite inertia and the convective transport of heat. Inclusion of these effects leads to deformation, and this subject has been studied generally for droplets asymptotically in Ca, Re and Pe by Bratukhin (1976), Thompson, DeWitt & Labus (1980), Balasubramanian & Chai (1987) and Hariri, Nadim & Borhan (1990). The effect of the convective transport of energy for the single fluid particle problem were studied for a spherical geometry (zero capillary number) and negligible inertia asymptotically for small Pe by Subramanian (1981, 1983) and numerically for order one Pe by Shankar & Subramanian (1988). These latter results established that the convective transport of energy reduces the surface temperature gradient on the fluid particle surface and thereby reduces the migration velocity. Recent advances on the single fluid particle problem have examined the retardation in thermocapillary migration owing to the adsorption of an insoluble surfactant monolayer on the drop surface (Kim & Subramanian 1989*a*, *b*; Nadim & Borhan 1989).

In terrestrial environments, the influence of the thermocapillary force on the motion of a fluid particle subject to a temperature gradient is usually unimportant because the magnitude of the thermocapillary force is much less than the gravitational force arising from particle–continuous phase density differences. However, thermocapillary forces can become dominant in microgravity environments, and the emergence of the possibility of fluids material processing in the reduced gravity environment of an orbiting spacecraft in near free-fall has focused increasing attention on thermocapillary migration of bubbles and drops. Some examples of materials processing where thermocapillary fluid particle migration is expected to play a significant role are the often cited high technology glass manufacture (Weinberg 1978) and miscibility gap alloy solidification (Bergman *et al.* 1982). As described by Weinberg (1978), high technology glass is most favourably manufactured from its melt in a containerless cooling process where impurities

cannot leach from the bounding container, and the container cannot serve as a site for heterogeneous nucleation. However, although a microgravity environment easily allows for such processing, bubbles created in the glass melt in the absence of buoyancy remain suspended and are incorporated in the final product. Thermocapillary migration has been suggested as a means for removal of these bubbles. In miscibility gap solidification, equilibrium liquid alloy mixtures consisting of droplets of one composition dispersed in a continuous phase of another can be formed because of the miscibility gap in the phase diagram. In the absence of buoyancy effects, cooling of this mixture can ultimately result in the formation of a composite solid material consisting of grains of one composition uniformly interspersed in a solid of another composition. However, the quality of the product will be affected by thermocapillary induced migrations which may reduce the uniformity of the grain structure.

To understand the behaviour of thermocapillary migrations in the more complex space processing applications where fluid particle swarms move in the vicinity of fluid or solid boundaries, it is necessary to begin to study and calculate in a fundamental way migration velocities of particles in the presence of the boundaries of other particles or walls. This is an involved subject because the migration velocity of a fluid particle in the presence of a boundary is determined not only by the hydrodynamic resistance the boundary offers to the forward motion of the particle, but also the corresponding thermal interactions between these bodies since these determine the temperature distribution on the fluid particle surface which drives the migration.

Fluid particle–particle, and fluid particle–wall boundary interactions in the context of thermocapillary migration have been studied for several geometries. Meyyappan, Wilcox & Subramanian (1981) examined the quasi-static movement of a spherical gas bubble perpendicular to an isothermal fluid or solid plane for zero Pe and Re. Solutions for the temperature isotherms demonstrated that the temperature gradient along the bubble surface decreases as the fluid particle approaches the wall. This behaviour, taken together with the increasing hydrodynamic retardation as the fluid particle approaches the wall, causes the migration velocity to decrease from the value in an infinite medium. Ascoli & Leal (1990) re-examined this problem for the case of order one capillary numbers and a solid surface, and found that bubble flattening as the fluid particle comes within a diameter or so of the wall causes the terminal velocity to be greater than the spherical value, but still less than the value in an infinite medium. The corresponding problem of a liquid drop of finite conductivity moving normal to a plane surface was studied by Barton & Subramanian (1990) and Chen & Keh (1990) for spherical bubbles and negligible inertia and thermal convection, and Ascoli & Leal (1990) under the same assumptions except allowing deformation. The results for the migration velocities can be significantly different from those for the migration of a bubble, and these differences illustrate the important role played by the thermal interaction. Both Barton & Subramanian and Chen & Keh determined that when the conductivity of the surrounding medium is less than the drop phase, the temperature gradient on the drop surface increases as the fluid particle approaches the wall. Both studies found that for the case of a fluid wall, as the droplet approaches the wall, the increase in the temperature gradient offsets the increasing hydrodynamic retardation, and the fluid particle velocity increases from its value in an unbounded region.

Other studies have examined problems similar to those above in which the hydrodynamic and thermal interactions occur normal to the direction of motion.

Meyyappan, Wilcox & Subramanian (1983) investigated numerically the rectilinear, quasi-static movement of two unequal sized spherical bubbles along their line of centres, again for negligible inertia and thermal convection. From the results, Meyyappan *et al.* developed a useful rule for approximately predicting the migration velocities for separation distances that are not very small compared to the fluid particle diameters, and this rule allows for a qualitative understanding of the thermal and hydrodynamic interaction for the two fluid particle case. For each sphere, the migration velocity may be approximately obtained by summing two terms. Consider the calculation for sphere a separated by a centre-to-centre distance d' from sphere b, with both spheres subject to a far-field temperature gradient $(\nabla' T')_\infty$. The first term in the approximation is the velocity of a owing to the streaming motion induced by the isolated migration velocity of b. The second is the thermocapillary migration velocity of a in an infinite medium subject to a far-field temperature gradient equal to the local gradient which exists a distance d from b, when b is isolated and subject to $(\nabla' T')_\infty$. Since, for a bubble, this local gradient is smaller than $(\nabla' T')_\infty$ owing to the distortion in the isotherm field caused by b, this elementary approximation for the thermal interaction reduces the motion of a relative to its value in an infinite medium. Meyyappan *et al.* found that for the smaller fluid particle, the streaming of the larger fluid particle acting on the smaller one overcompensates for the reduction in the terminal velocity owing to the thermal interaction, and the fluid particle moves faster than when isolated. For the larger fluid particle, since the streaming motion due to the smaller fluid particle is not as large, the thermal interaction dominates and slows the fluid particle down from the infinite medium value. For equal sized spheres, these effects cancel in this approximation, and the fluid particles move with isolated velocities, a result confirmed for all separation distances numerically by Meyyappan *et al.* and analytically by Feuillebois (1989). This heuristic approximation has also been used in studying the normal interaction problem of the eccentric thermocapillary migration of a bubble moving in a spherical drop along whose surface a temperature gradient is imposed (Shankar, Cole & Subramanian 1981; Annamalai *et al.* 1982; Shankar & Subramanian 1983). This eccentric motion was reconsidered by Morton, Subramanian & Balasubramaniam (1990) for the more general case in which the inside fluid particle is a drop, and the outside drop is placed in a temperature gradient and its surface temperature is determined by solving the conduction problem of one drop embedded inside another. The problem of two gas bubbles moving rectilinearly along their line of centres has been generalized to include the influence of droplet viscosity in an exact treatment by Keh & Chen (1990). Meyyappan & Subramanian (1984), using a far-field technique, constructed approximate solutions for the thermocapillary motion of two bubbles moving with an arbitrary orientation with respect to each other. Anderson (1985) reconsidered this problem for the case of droplets, and constructed approximate solutions using the method of reflections.

The aim of this paper is to examine lateral boundary interactions in thermocapillary migration by studying theoretically the movement of a drop situated in a liquid-filled tube and subject to an axial temperature gradient. The simplest case is adopted of a spherical drop in steady, axisymmetric, inertialess motion along the tube centreline. Thermal convection is neglected, and the tube wall is assumed to be insulated. The assumption that the fluid particle remains spherical requires that tractions which are exerted on the fluid particle by the continuous phase, and which tend to deform the drop and stretch it in the flow direction, are much smaller than the effects of surface tension forces which tend to keep the drop spherical. The ratio

of the magnitudes of these distorting tractions to the force of surface tension is the capillary number, and is defined here as $\mu'^{(2)}U'/\sigma'$, where U' is the fluid particle velocity, $\mu'^{(2)}$ is the continuous phase viscosity and σ' is the interfacial tension between the droplet and continuous phases. This number must remain much smaller than one in order for the fluid particle to retain a spherical shape. The deformation will follow that which has been generally observed for the motion, at low capillary number, of fluid particles in a tube owing to an external applied force or a far-field Poiseuille flow (Wang & Skalak 1969; Martinez & Udell 1990). The drop elongates in the direction of the flow, and develops a tail at the trailing edge. Distortions from a spherical shape at low capillary number in thermocapillary migration have been examined by Ascoli & Leal (1990) for the case of migration towards a plane wall.

There are several reasons for undertaking this investigation. First are the obvious applications to fluids material space processing involving bubble or drop motion in cylindrical geometries such as solid-walled tubes and containerless liquid filaments. The operations of the space vehicles themselves can also involve directly the motion of fluid particles in tubes, as, for example, the presence and movement of bubbles in fuel lines. (In this case, however, the present analysis may be only qualitatively useful since Reynolds and thermal Péclet numbers may not be small owing to the effects of imposed flows.) More importantly, results from this study are a necessary first step in developing cylindrically symmetric, periodic array type theories for the motion of droplet swarms. Finally, by taking the tube wall to be insulated and neglecting thermal convection, the posed problem represents an excellent model for studying the competition between strong thermal and relatively weak hydrodynamic wall–fluid particle lateral interactions. Since the tube wall is insulated, axial conduction around a fluid particle of relatively low conductivity will generate large temperature gradients on the fluid particle surface. These gradients will enhance the migration velocity, although their action will be retarded by the hydrodynamic interaction of the fluid particle with the tube wall. The thermal enhancement and hydrodynamic resistance increase as the sphere to tube diameter increases. Resolving which effect is overriding at small particle–wall gap thicknesses is a central goal of this study, and is an important question to resolve before determining migrations of closely packed bubble swarms.

For lateral motion, this question of competition between thermal and hydrodynamic interaction has not been fully examined. Meyyappan & Subramanian (1987) studied the motion of a spherical bubble parallel to a plane solid wall for negligible inertia and thermal convection, and found that the velocity decreased relative to the isolated value for parallel motions close to the wall. In this case resistance to heat transfer through the particle–surface gap should enhance the migration velocity. Nevertheless, the result indicates that the hydrodynamic resistance is overriding. It should be noted, however, that the far-field temperature gradient was imposed on the wall. Hence the wall was not insulated, and therefore heat can be conducted through it. In addition much of the energy can be conducted around the side of the fluid particle away from the wall rather than through the gap. Both of these factors act to reduce the surface temperature gradient and explain the dominance of hydrodynamic resistance. The tube geometry adopted in this study, because it does not have these mitigating factors, is a more appropriate model for assessing strong thermal interaction. The only study undertaken for thermocapillary migration in a cylindrical geometry was that of Hasan & Balasubramaniam (1989), who studied the motion of a long gas slug in an isothermal tube owing to an axial temperature gradient. An approximate solution for the migration velocity was obtained based on

a lubrication solution of the hydrodynamic equations in the thin-film region surrounding the cylindrical portion of the bubble, and an overall force balance to calculate the pressure gradient in the film. The approximate result for the migration velocity decreases as the gap thickness between the slug and the tube wall decreases, again indicating the dominance of hydrodynamic interaction for the isothermal wall case.

This paper is divided into three major sections. In the first (§2), the fluid mechanical and thermal field and boundary equations are detailed (§2.1), and the numerical solution technique is described (§§2.2 and 2.3). Numerical solutions are obtained by a boundary collocation procedure (Leichtberg, Pfeffer & Weinbaum 1976) in which general analytical solutions to the Stokes and Laplace equations which satisfy the tube-wall conditions exactly are developed, and made to satisfy the fluid–particle surface conditions at discrete points on the surface. The results are detailed in §3 in three parts. The first (§3.1) presents the solutions for the conduction problem in terms of temperature isotherms, and graphs of the surface temperature distribution and pole temperature difference. The second section describes hydrodynamic results. This linear-Stokes-flow problem is separable into two fixed-fluid particle flow idealizations, one in which a uniform flow from infinity streams over the fluid particle in the absence of a thermocapillary force, and a second in which the thermocapillary stress causes fluid streaming in closed convection cells with no flow far away from the particle. Each idealization contributes a force on the particle, and in §3.2, these forces are described as a function of force coefficients which are presented graphically in terms of the conductivity and viscosity particle–continuous phase ratios, and the sphere to tube diameter quotient. The terminal velocity relative to that of an isolated fluid particle is determined by the ratio of the force coefficients, and in §3.3 the relative velocity is detailed as a function of the fluid particle to tube diameter ratio and conductivity and viscosity ratios. From these results, conclusions are drawn as to whether thermal or hydrodynamic effects become overriding as the gap thickness decreases. The paper ends with a summary (§4).

2. Formulation and solution procedure

2.1. *Thermal and hydrodynamic field equations and boundary conditions*

The problem is formulated in a reference frame which is fixed to the particle, and which is therefore moving with a uniform velocity U' relative to the stationary laboratory frame. In this paper, dimensional quantities are marked by a prime, and dimensionless quantities are unprimed. In the moving frame, cylindrical (ρ', ω, z') and spherical coordinates (r', θ, ϕ) are located with the origins of both systems taken to be at the fluid particle centre, and the z'-axis of the cylindrical system coincident with the tube centreline (see figure 1). Note that in this fluid particle fixed frame the wall is moving in the z'-direction with velocity $-U'$. The radius of the fluid particle and of the tube are denoted, respectively, by a' and b'. Droplet and continuous phase variables are denoted by superscripts (1) and (2) respectively. Finally, viscosities and thermal conductivities are denoted by $\mu'^{(i)}$ and $k'^{(i)}$, and the ratios of the droplet to the continuous phase viscosity and conductivities are denoted by κ and k respectively. The temperature gradient is imposed in the laboratory frame. Far from the drop, in the lab frame, the temperature field is of the form $T'(\zeta') = (\nabla' T')_\infty \zeta' + T'_0$, where T' denotes the temperature, $(\nabla' T')_\infty$ denotes the imposed gradient, and ζ' is the lab frame cylindrical axial coordinate. This coordinate is related to the fluid particle fixed axis coordinate z' by $z' = \zeta' - U't'$. Thus in the moving frame the temperature

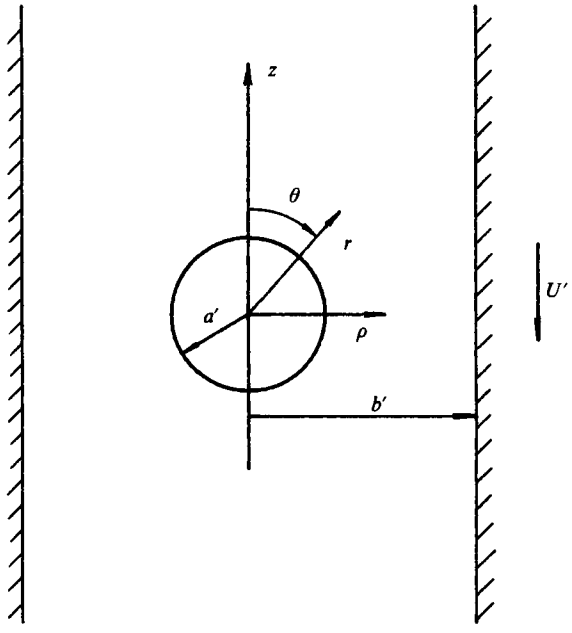

FIGURE 1. Definition sketch of the thermocapillary movement of a fluid particle of radius a' translating axisymmetrically in an insulated tube of radius b'. The illustration is in a reference frame moving with the fluid particle velocity U', and spherical and polar coordinates, with origins fixed to the particle, are defined as shown.

field far from the drop is given by $T'(z') = (\nabla' T')_\infty z' + (\nabla' T') U' t' + T'_0$. The dependence of the surface tension σ' on the temperature is assumed to be linear, and the constant gradient is denoted by $\partial\sigma'/\partial T'$. Non-dimensionalizations are formulated using the following scalings: spatial coordinate variables r', z' and ρ' are scaled by the fluid particle radius a'; velocities are scaled by U'_0, the terminal velocity for the case in which the walls are infinitely far away and the fluid particle therefore translates in an infinite medium. This velocity is given by Young *et al.* (1959) as

$$U'_0 = -\frac{a'(\partial\sigma'/\partial T')'(\nabla' T')_\infty}{\mu'^{(2)}(1+\frac{3}{2}\kappa)(2+k)}. \tag{1}$$

A non-dimensional temperature field $\Theta^{(i)}(z,\rho)$ measured in the moving system is defined as:

$$\Theta^{(i)}(z,\rho) = (T'^{(i)}(z,\rho) - (\nabla' T')_\infty U' t' - T'_0)/(a'(\nabla' T')_\infty).$$

Note that this field must tend to $\pm z$ as $z \to \pm\infty$. When the thermal equations are cast in non-dimensional form using $\Theta^{(i)}(z,\rho)$, it can easily be shown that $\Theta^{(i)}(z,\rho)$ is antisymmetric with respect to z for all ρ. Therefore $\Theta^{(i)}(z=0,\rho) = 0$ and the dimensional temperature along the equatorial plane is equal to $(\nabla' T')_\infty U' t' + T'_0$. Since the non-dimensional temperature field is antisymmetric with respect to z, the Marangoni force, which is proportional to $(\partial\Theta^{(i)}/\partial\theta)(r=1) = \cos\theta\,(\partial\Theta^{(i)}/\partial\rho)(r=1) - \sin\theta\,(\partial\Theta^{(i)}/\partial z)(r=1)$ is an even function of z. Hence the velocity field is symmetric with respect to the sphere equator: $V^{(i)}_\rho(\rho,z) = -V^{(i)}_\rho(\rho,-z)$, and $V^{(i)}_z(\rho,z) = V^{(i)}_z(\rho,-z)$.

In formulating the energy conservation equations, thermal convection is neglected

under the assumption of small Péclet number, and Laplace's equation describes the temperature field at steady state:

$$\nabla^2\Theta^{(i)} = 0. \tag{2}$$

The boundary conditions on the temperature fields are as follows:

(i) The tube wall, $\rho = b'/a'$, is insulated:

$$\frac{\partial\Theta^{(2)}}{\partial\rho} = 0. \tag{3}$$

(ii) At the bubble surface, $r = 1$, the heat flux and temperature are continuous across the interface:

$$k\frac{\partial\Theta^{(1)}}{\partial r} = \frac{\partial\Theta^{(2)}}{\partial r}, \tag{4}$$

$$\Theta^{(1)} = \Theta^{(2)}. \tag{5}$$

(iii) Far from the bubble, the temperature field in the continuous phase is linear in z:

$$\lim_{|z|\to\infty}\Theta^{(2)} = z. \tag{6}$$

(iv) At the centre of the sphere ($r = 0$), the temperature is finite.

Since the hydrodynamic flow is axisymmetric and the fluids incompressible, non-dimensional velocities may be expressed in terms of a non-dimensional stream function $\psi^{(i)}$ ($\psi^{(i)} = \psi'^{(i)}/(a'^2U_0')$). Two representations of $\psi^{(i)}$ are used, one in terms of cylindrical coordinates (ρ, z) and one in terms of spherical coordinates (r, θ). These representations are related to the velocity fields as expressed in the respective systems by the following relations:

$$V_r^{(i)} = -\frac{1}{r^2\sin\theta}\frac{\partial\psi^{(i)}}{\partial\theta}, \quad V_\theta^{(i)} = \frac{1}{r\sin\theta}\frac{\partial\psi^{(i)}}{\partial r}, \tag{7}$$

$$V_z^{(i)} = -\frac{1}{\rho}\frac{\partial\psi^{(i)}}{\partial\rho}, \quad V_\rho^{(i)} = \frac{1}{\rho}\frac{\partial\psi^{(i)}}{\partial z}. \tag{8}$$

For steady, creeping flows the Navier–Stokes equations in terms of the stream function is of the form

$$E^2(E^2\psi^{(i)}) = 0, \tag{9}$$

where E^2 is the axisymmetric stream function operator. The definitions of this operator in cylindrical and spherical coordinates is given in Happel & Brenner (1973).

For the velocity field the boundary conditions are:

(i) At the bubble centre

$$\lim_{r\to0} V_r^{(1)} \quad \text{and} \quad \lim_{r\to0} V_\theta^{(1)} \quad \text{exist.} \tag{10}$$

(ii) Far from the bubble, the velocity field is uniform

$$\lim_{|z|\to\infty} V_z^{(2)} = -U \tag{11}$$

where U is the non-dimensional velocity of the fluid particle ($U = U'/U_0'$).

(iii) At the tube wall, $\rho = b'/a'$, the velocity is equal to the wall velocity:

$$V_z^{(2)} = -U, \tag{12}$$

$$V_\rho^{(2)} = 0. \tag{13}$$

(iv) At the surface of the bubble ($r = 1$) velocities are continuous, the normal velocity is equal to zero and the difference in tangential shear stresses is balanced by the Marangoni force:

$$V_\theta^{(1)} = V_\theta^{(2)}, \tag{14}$$

$$V_r^{(1)} = V_r^{(2)} = 0, \tag{15}$$

$$\left(\frac{\partial V_\theta^{(2)}}{\partial r} - \frac{V_\theta^{(2)}}{r}\right) - \kappa\left(\frac{\partial V_\theta^{(1)}}{\partial r} - \frac{V_\theta^{(1)}}{r}\right) = (1+\tfrac{3}{2}\kappa)(2+k)\frac{\partial \Theta^{(2)}}{\partial \theta}. \tag{16}$$

It is important to note that since the tangential stress balance equation (16) has been non-dimensionalized using the infinite medium migration velocity (equation (1)), which itself is proportional to the constant surface tension gradient $\partial\sigma'/\partial T'$, the non-dimensional tangential stress balance becomes independent of this gradient.

2.2. *Solution for the temperature field*

Owing to the neglect of convection, the energy equations (2)–(6) are independent of the velocity field, and may therefore be solved independently. In the fluid particle interior, the general solution to Laplace's equation which is bounded at the origin (cf. consideration (iv) after equation (6)) may be formulated as an infinite series in Legendre polynomials. Since the temperature field is antisymmetric with respect to z, only odd Legendre polynomials are included in the series summation. Therefore:

$$\Theta^{(1)}(r,\theta) = \sum_{n=1}^{\infty} A_n P_n(\cos\theta)\, r^n \quad (n \text{ odd}), \tag{17}$$

where $P_n(\cos\theta)$ denote the Legendre functions.

For the continuous phase, a general solution to Laplace's equation for $\Theta^{(2)} - z$ can be constructed by the addition of the general integral solution in cylindrical coordinates which is bounded as $\rho \to 0$, tends to zero as $z \to \pm\infty$ and is odd in z, and the spherical coordinate solution which also disappears as $r \to \infty$ and is antisymmetric in θ with respect to $\frac{1}{2}\pi$:

$$\Theta^{(2)}(\rho,z,r,\theta) = \int_0^\infty C(t) I_0(t\rho) \sin tz\, \mathrm{d}t + \sum_{n=1}^{\infty} B_n P_n(\cos\theta)\, r^{-(n+1)} + z \quad (n \text{ odd}), \tag{18}$$

where I_0 is the modified Bessel functions of the first kind, and the restriction to odd indices in the Legendre expansion is due to the antisymmetry of the temperature field. Note that this construction satisfies the boundary condition at infinity (equation (6)).

The technique used to obtain, from the boundary conditions (3)–(5), the constants A_n and B_n in the Legendre expansions and the function $C(t)$ in the integral solution is described as follows. First, the zero flux boundary condition on the tube wall is satisfied exactly by using a Fourier sine inversion to solve for the unknown function $C(t)$ in terms of a Legendre expansion of the B_n constants. Secondly, a multipole collocation technique is used to satisfy the boundary conditions on the surface of the drop.

The spherical coordinates in the exterior phase solution may be rewritten in terms of cylindrical coordinates by using the transformations $\theta(\rho,z) = \mathrm{Arctan}\,(\rho/z)$ $(0 \leqslant$

$\theta < \pi$), $\cos\theta = z/(\rho^2+z^2)^{\frac{1}{2}}$ and $r = (\rho^2+z^2)^{\frac{1}{2}}$. By using this transformation in (18), the zero-flux boundary condition may be written in the form:

$$0 = \frac{\partial \Theta^{(2)}}{\partial \rho}(\rho = R) = \int_0^\infty tC(t)\, I_1(tR) \sin tz \, dt + \sum_{m=1}^{\infty} B_n \frac{\partial}{\partial \rho}\left[P_n\left\{\frac{z}{(\rho^2+z^2)^{\frac{1}{2}}}\right\}(\rho^2+z^2)^{-\frac{1}{2}(n+1)}\right]\Bigg|_{\rho=R} \quad (n = \text{odd}). \tag{19}$$

In the above, the ratio b'/a' is denoted by R. The function $C(t)$ may be obtained from (19) by inverting and then integrating the inverse integral. The result is:

$$C(t)\, tI_1(Rt) = -\sum_{n=1}^{\infty} B_n \frac{\partial}{\partial \rho}[Q_n(\rho, t)]|_{\rho=R} \tag{20}$$

where $$Q_n = \frac{2}{\pi}\int_0^\infty P_n\left\{\frac{z}{(\rho^2+z^2)^{\frac{1}{2}}}\right\}(\rho^2+z^2)^{-\frac{1}{2}(n+1)} \sin tz \, dz.$$

Integrating the above (Leichtberg *et al.* 1976) yields:

$$Q_n = (-1)^{\frac{1}{2}(n-1)} \frac{2}{\pi n!} t^n K_0(\rho t),$$

and K_0 is a modified Bessel function of the second kind. By differentiating Q_n with respect to ρ a final expression for $C(t)$ may be obtained:

$$C(t) = \sum_{n=1}^{\infty} B_n \, T_n(Rt),$$

where $T_n = (-1)^{\frac{1}{2}(n-1)}(2/\pi n!)\, t^n K_1(Rt)/I_1(Rt)$. For a fixed t, the above series for $C(t)$ rapidly converges because of the $n!$ in the denominator.

Substituting this solution for $C(t)$ into (18) allows for the representation of the exterior phase solution to be written in the form:

$$\Theta^{(2)}(r, \theta) = \sum_{n=1}^{\infty} B_n \int_0^\infty T_n(Rt)\, I_0(tr \sin\theta) \sin(tr\cos\theta)\, dt + \sum_{n=1}^{\infty} B_n P_n(\cos\theta)\, r^{-(n+1)} + r\cos\theta \quad (n = \text{odd}). \tag{21}$$

The thermal boundary conditions at the sphere surface $r = 1$ (equations (4) and (5)) can be applied directly to the solution forms given by (17) and (21):

$$k\sum_{m=1}^{\infty} A_m \, m P_m(\cos\theta) = \cos\theta - \sum_{m=1}^{\infty} B_m(m+1) P_m(\cos\theta) + \sum_{m=1}^{\infty} B_m \int_0^\infty T_m(Rt)\, tI_1(t\sin\theta) \sin(t\cos\theta)\sin\theta \, dt + \sum_{m=1}^{\infty} B_m \int_0^\infty T_m(Rt)\, tI_0(t\sin\theta)\cos(t\cos\theta)\cos\theta \, dt, \tag{22}$$

$$\sum_{m=1}^{\infty} A_m P_m(\cos\theta) = \cos\theta + \sum_{m=1}^{\infty} B_m P_m(\cos\theta) + \sum_{m=1}^{\infty} B_m \int_0^\infty T_m(Rt)\, I_0(t\sin\theta)\sin(t\cos\theta)\, dt. \tag{23}$$

The above two equations are in terms of the remaining unknown infinite sets of constants, A_m and B_m. It is important to note that when the expression for $T_m(Rt)$ is inserted into the improper integrals appearing in the above two equations, the resulting integrands can easily be shown to be of order $t^{m+\frac{1}{2}}e^{t(\sin\theta-2R)}$ (for (22)) or $t^{m-\frac{1}{2}}e^{t(\sin\theta-2R)}$ (for (23)) as $t\to\infty$ and are bounded as $t\to 0$. Because of these properties, the improper integrals are readily seen to be convergent. Numerical integration was undertaken by using the integration package DQDAG from the IMSL Math Library. This routine only accepts numerical values for the upper and lower limits. The lower limit was set equal to a value of 10^{-8}. A sufficiently large value of the upper limit was found so that for values larger than this one, the change in the value of the integral was negligible. The contribution from 0 to the lower limit was then estimated using asymptotic formulae for the integrand as $t\to 0$, and this estimate was then checked against the value of the integral to confirm that it was a small contribution.

The constants A_m and B_m are determined from (22) and (23) by a multipole collocation technique in which these equations are satisfied at M discrete points on the sphere surface, and the summations in the equations are truncated so as to include terms up to B_{2M-1} and A_{2M-1}. The result is a set of $2M$ linear equations in terms of $2M$ constants which can be cast in the following way:

$$k\sum_{m=1}^{2M-1}\{A_m mP_m(\cos\theta_i)+B_m[(m+1)P_m(\cos\theta_i) - \int_0^\infty T_m(Rt)\,tI_1(t\sin\theta_i)\sin(t\cos\theta_i)\sin\theta_i\,\mathrm{d}t - \int_0^\infty T_m(Rt)\,tI_0(t\sin\theta_i)\cos(t\cos\theta_i)\cos\theta_i\,\mathrm{d}t]\} = \cos\theta_i, \quad (24)$$

$$\sum_{m=1}^{2M-1}\{A_m P_m(\cos\theta_i) - B_m[P_m(\cos\theta_i) + \int_0^\infty T_m(Rt)\,I_0(t\sin\theta_i)\sin(t\cos\theta_i)\,\mathrm{d}t]\} = \cos\theta_i, \quad (25)$$

where i denotes the collocation point ($i = 1, 2, \ldots, M$). Note that because of the antisymmetry, collocation points need only be taken along the first quadrant of the sphere. The above set can be solved by matrix inversion to yield values for the constants A_m and B_m up to index $2M-1$. As M is increased sufficiently, the values obtained for A_m and B_m by inversion of matrices of higher rank begin to converge, and the truncated expressions for the temperature field approach the exact solution.

In this implementation of the collocation technique, the convergence criteria is based on incrementing M until a prescribed resolution is achieved for the temperature gradient on the surface of the drop. At the level M, this gradient is given by the truncated expression:

$$\frac{\partial\Theta^{(1)}}{\partial\theta}(1,\theta_i) = \sum_{m=1}^{2M-1} A_m[mzP_m(z) - mP_{m-1}(z)]/\sin\theta_i. \quad (26)$$

Convergence is formulated in this way because the gradient in the surface temperature is what determines directly the hydrodynamic flow field and terminal velocity. At each level in M, the surface temperature gradient is evaluated from the truncated expression at three degree intervals along the first quadrant of the drop from $\theta = 0$. These values are then compared with the surface temperature gradient at the same points on the sphere surface for the level $M-1$, and the gradient field is deemed converged when the difference at each angular location is less than $10^{-5}\%$.

λ	a'/b'	0.1	0.2	0.3	0.4	0.5	0.6	0.7	0.8	0.9
	M	4	6	6	6	8	10	12	14	16
λ_u	P	4	4	5	7	7	9	10	11	13
λ_m	L	3	3	4	4	4	5	5	6	7

TABLE 1. The number of collocation points necessary to achieve the accuracy requirement for the gas bubble ($\kappa = 0$ and $k = 1.0 \times 10^{-5}$)

Example values of M necessary to satisfy this criteria are given on the first row in table 1 as a function of a'/b' for $k = 1.0 \times 10^{-5}$. Note that as the ratio of the sphere to the tube diameter increases, M increases. As will be discussed in §3, for this case of a non-conducting sphere, the surface temperature gradient strongly increases with θ in the first quadrant as heat is conducted through the narrow gap between the sphere and tube wall, and more terms in the series expansion are necessary to describe this behaviour.

Some final notes with regard to the implementation of the collocation procedure: an examination of the linear algebraic equations (24) and (25) shows that when the collocation points $\theta_i = 0$ and $\frac{1}{2}\pi$ are used the equations become linearly dependent. In order to overcome this difficulty, these points can be replaced by closely adjacent points, i.e. $\theta_i = 0 - \epsilon$ and $\theta_i = \frac{1}{2}\pi - \epsilon$. The optimum value of ϵ is 0.8° as established by Leichtberg *et al.* (1976).

2.3. *Solution of the velocity field*

A general solution for the stream function of the droplet phase in spherical coordinates in which velocities are bounded at the drop centre (consideration (i) preceding equation (11)) may be expressed in terms of an infinite series of Gegenbauer polynomials $C_n^{-\frac{1}{2}}(\cos\theta)$:

$$\psi^{(1)}(r,\theta) = \sum_{n=2}^{\infty} (E_n^{(1)} r^n + F_n^{(1)} r^{n+2}) C_n^{-\frac{1}{2}}(\cos\theta) \quad (n = \text{even}), \tag{27}$$

where the restriction to even terms is a consequence of the flow field symmetry about the equatorial plane. For the continuous fluid, note first that the stream function must from (12) tend to $\frac{1}{2}U\rho^2$ as $|z| \to \infty$ in order to match to the uniform flow. Denoting this uniform flow field by $\psi_\infty(\rho)$, solutions for $\psi^{(2)} - \psi_\infty(\rho)$ must tend to zero as $|z| \to \infty$. General solutions which obey this far-field restriction may be constructed by the addition of the general cylindrical solution which is bounded as $\rho \to 0$ and tends to zero as $|z| \to \infty$ and the spherical solution which disappears as $r \to \infty$:

$$\psi^{(2)} = \psi_\infty(\rho) + \int_0^\infty [A(t)\,\rho I_1(t\rho) + B(t)\,\rho^2 I_0(t\rho)] \cos tz \, dt + \sum_{n=2}^{\infty} (E_n^{(2)} r^{-n+1} + F_n^{(2)} r^{-n+3}) C_n^{-\frac{1}{2}}(\cos\theta) \quad (n \text{ even}). \tag{28}$$

As was the case with the solution for the temperature field, the determination of the hydrodynamic constants and functions is undertaken by a two-step procedure in which the wall conditions are satisfied exactly by a Fourier inversion, and the conditions on the fluid particle surface are satisfied numerically at collocation points.

The boundary conditions on the surface of the tube are given by (12)–(13); in order to satisfy these conditions, explicit expressions for the velocity fields in the

cylindrical system for the solution form given by (28) are given first with the aid of the spherical–cylindrical coordinate transformation:

$$V_z(z,\rho) = -\frac{1}{\rho}\frac{\partial \psi_\infty}{\partial \rho} - \int_0^\infty \{A(t)\,tI_0(t\rho) + B(t)[\rho t I_1(t\rho) + 2I_0(t\rho)]\}\cos(tz)\,\mathrm{d}t - \sum_{n=2}^{\infty}[E_n^{(2)}G_n^1(\rho,z) + F_n^{(2)}G_n^2(\rho,z)], \quad (29a)$$

$$V_\rho(z,\rho) = \int_0^\infty [A(t)\,I_1(t\rho) + B(t)\,\rho I_0(t\rho)]\,t\sin(tz)\,\mathrm{d}t + \sum_{n=2}^{\infty}[E_n^{(2)}G_n^5(\rho,z) + F_n^{(2)}G_n^6(\rho,z)], \quad (29b)$$

where the functions $G_n^k(\rho,z)$ appearing in the above are detailed in the Appendix. From (12) and (29a) the following equation is obtained:

$$\int_0^\infty \{A(t)\,tI_0(Rt) + B(t)[RtI_1(Rt) + 2I_0(Rt)]\}\cos(tz)\,\mathrm{d}t = -\sum_{n=2}^{\infty}[E_n^{(2)}G_n^1(R,z) + F_n^{(2)}\,G_n^2(R,z)]. \quad (30)$$

From (13), it is clear that the stream function at the wall is a constant; from the solution form of (28) this constant is clearly equal to $\psi_\infty(\rho = R)$ and the integral and series summations must equal zero:

$$\int_0^\infty [A(t)\,RI_1(Rt) + B(t)\,R^2 I_0(Rt)]\cos(tz)\,\mathrm{d}t = -\sum_{n=2}^{\infty}[E_n^{(2)}G_n^3(R,z) + F_n^{(2)}G_n^4(z)]. \quad (31)$$

By applying Fourier cosine integral inversions to (30) and (31), $A(t)$ and $B(t)$ can be expressed in terms of the constants $E_n^{(2)}$ and $F_n^{(2)}$ as follows:

$$\left.\begin{aligned} A(t)\,tI_0(Rt) + B(t)[RtI_1(Rt) + 2I_0(Rt)] &= -\sum_{n=2}^{\infty}[E_n^{(2)}H_n^1(t) + F_n^{(2)}H_n^2(t)] \\ A(t)\,RI_1(Rt) + B(t)\,R^2 I_0(Rt) &= -\sum_{n=2}^{\infty}[E_n^{(2)}H_n^3(t) + F_n^{(2)}H_n^4(t)], \end{aligned}\right\} \quad (32)$$

where the functions $H_n^i(t)$, $i = 1,2,3,4$, are obtained by analytical integration (Leichtberg *et al.* 1976) and are detailed in the Appendix. The integrals which define the $H_n^i(t)$ functions are, like the corresponding conduction integrals, improper and divergent at the lower (zero) limit. However, by using asymptotic formulae, the divergence can be shown to be integrable, and the improper integral is convergent. In the numerical solution to follow, these integrals were once again evaluated using the IMSL's DQDAG routine, and the integral limits were specified in a manner which was similar to that used for the conduction integrals.

From (32), $A(t)$ and $B(t)$ can be solved in terms of the unknown constants $E_n^{(2)}$ and $F_n^{(2)}$. Substituting this solution into (28), the stream function can be expressed in spherical coordinates r,θ in terms only of $E_n^{(2)}$ and $F_n^{(2)}$:

$$\psi^{(2)}(r,\theta) = \psi_\infty(r,\theta) + \sum_{n=2}^{\infty}[E_n^{(2)}S_n^1(r,\theta) + F_n^{(2)}S_n^2(r,\theta)], \quad (33)$$

where the functions S_n^q are given in the Appendix.

Four unknown constants remain to be determined, $E_n^{(1)}$, $F_n^{(1)}$, $E_n^{(2)}$, and $F_n^{(2)}$. Of the two pertaining to the solution for the drop stream function, one constant can be expressed in terms of the other by the condition that $V_r^{(1)}(r=1,\theta)=0$. Eliminating $F_n^{(1)}$ in this manner, the inner solution can be expressed as:

$$\psi^{(1)}(r,\theta)=\sum_{n=2}^{\infty}E_n^{(1)}(r^n-r^{n+2})C_n^{-\frac{1}{2}}(\cos\theta). \tag{34}$$

By using the remaining hydrodynamic boundary conditions on the sphere surface, three simultaneous equations are obtained:

$$\left.\begin{aligned}
-U\cos\theta &= \sum_{n=2}^{\infty}[E_n^{(2)}S_n^3(1,\theta)+F_n^{(2)}S_n^4(1,\theta)],\\
-U\sin\theta &= \sum_{n=2}^{\infty}[E_n^{(2)}S_n^5(1,\theta)+F_n^{(2)}S_n^6(1,\theta)+\frac{2}{\sin\theta}E_n^{(1)}C_n^{-\frac{1}{2}}(\cos\theta)],\\
-U\sin\theta+(2+k)(1+\tfrac{3}{2}\kappa)\frac{\partial\Theta}{\partial\theta}(1,\theta) &= \sum_{n=2}^{\infty}[E_n^{(2)}S_n^7(1,\theta)+F_n^{(2)}S_n^8(1,\theta)\\
&\quad -\frac{2(2n-1)\kappa}{\sin\theta}E_n^{(1)}C_n^{-\frac{1}{2}}(\cos\theta)].
\end{aligned}\right\} \tag{35}$$

The above equation set contains the remaining three infinite series of unknown constants, $E_n^{(2)}$, $F_n^{(2)}$ and $E_n^{(1)}$. Solutions for these constants from the above three equations are obtained by the same collocation procedure used for the temperature field, but there are a few important differences. Since the inhomogeneity in the above three equations consists of two separate terms, one a multiple of U and one a multiple of the fluid particle surface temperature gradient, the solutions for the constants may be decomposed into separate terms, one in which $(\partial\Theta/\partial\theta)(1,\theta)=0$ and U is non-zero, and one in which $U=0$ and the temperature gradient is non-zero. This decomposition reflects the linearity of the Stokes equations and boundary conditions. It also allows for the interpretation of the fluid particle movement due to the temperature gradient as the sum of two flow idealizations in the fluid particle fixed frame, one in which the temperature gradient is equal to zero and a uniform flow from infinity moves over the fluid particle (U not equal to zero), and a second idealization in which the flow at infinity is zero, and a temperature gradient produces fluid streaming.

The values for the constants for the first case of uniform flow are linear in U, and may therefore be solved generally by setting $U=1$. These constants are denoted with a U subscript. As before, a collocation solution procedure is developed in which the above three equations are satisfied at P points on the first quadrant, the infinite series are truncated at $n=2P$, and the $3P$ constants are obtained from the algebraic solution of the satisfaction of the three boundary conditions at P collocation points. The convergence criteria is formulated in the following way. It will be shown in the next section that (i) the terminal velocity is determined by the sum of the hydrodynamic forces exerted by the continuous phase on the fluid particle in the two flow idealizations, and (ii) this force is only dependent on $F_2^{(2)}$. Since the aim of the study is the accurate computation of the terminal velocity, the convergence criteria is based on the accurate resolution of $F_2^{(2)}$. Thus the constant $F_{2U}^{(2)}$ is computed for $P-1$ and P collocation points, and the relative change in the constant is then obtained. The collocation number is incremented until the relative change is less than 10^{-5}.

Listed on the second line of table 1 are the values of P necessary for convergence for $\kappa = 0$ as a function of a'/b'. The table indicates that the number of collocation points increases as the sphere to tube diameter increases. Although the hydrodynamic flow patterns will be examined carefully in the results section to follow, this trend is clearly a consequence of the fact that large θ-gradients in $V_\theta^{(2)}$ develop in the gap as a'/b' increases in order to keep the overall flow rate in the z-direction constant, and more terms in the series expansion are necessary to describe accurately these gradients.

In the second flow idealization, the fluid at infinity is at rest, and flow is only caused by the temperature gradient. Again using a collocation procedure for numerical solution, the constants are determined by truncating the infinite series at L terms and satisfying the three boundary conditions at L discrete points. (These constants are identified by an M subscript.) Convergence is based on the accurate determination of $F_{2M}^{(2)}$, and the number of collocation points L necessary to achieve a 10^{-5} resolution in this constant are given in the third line of table 1 for $\kappa = 0$ and $k = 1.0 \times 10^{-5}$. The table shows that more collocation points are necessary as the sphere to tube diameter increases. As will become clearer below, this trend results from the fact that the fluid streaming due to the Marangoni force creates recirculating eddies between the sphere and the tube wall, and as a'/b' increases these eddies are squeezed and large θ gradients develop which necessitate more terms in the series expansion.

3. Results and discussion

3.1. *Temperature field*

Three separate presentations are given to illustrate the results for the non-dimensional temperature field $\Theta^{(i)}(\rho, z)$, and the dependence of this field on the thermal conductivity and fluid particle to tube diameter ratios k and a'/b'. In the first presentation the temperature field isotherms are detailed. These are shown for the infinite system ($a'/b' = 0$) in figures 2(*a*) ($k = 1.0 \times 10^{-5}$) and 2(*b*) ($k = 5$), for $a'/b' = 0.5$ in figures 3(*a*) ($k = 1.0 \times 10^{-5}$) and 3(*b*) ($k = 5$) and for $a'/b' = 0.9$ in figures 4(*a*) ($k = 1.0 \times 10^{-5}$ and 4(*b*) ($k = 5$). The thermocapillary velocity is determined by the magnitude of the surface temperature gradient, $(\partial\Theta/\partial\theta)(r = 1, \theta)$. The final two presentations quantify this gradient by providing two different measures of $(\partial\Theta/\partial\theta)(r = 1, \theta)$. In figures 5 (for $a'/b' = 0.5$) and 6 ($a'/b' = 0.9$), $(\partial\Theta/\partial\theta)(r = 1, \theta)$ is plotted, as a function of θ, for different values of k. To facilitate comparison with the surface temperature gradient for an infinite continuous phase, plotted alongside the tube results in figures 5 and 6 are the infinite system gradients for the same value of k. In the second measure, the overall change in the surface temperature of a bounded droplet relative to the unbounded one is computed. This ratio is defined by Φ, and is given by:

$$\Phi = (\Theta(r = 1, \theta = 0) - \Theta(r = 1, \theta = \pi))(2 + k)/6, \tag{36}$$

where, for the case of an infinite continuous phase, the difference between the temperatures at the two poles is given by $6/(2+k)$, and is obtained from the surface temperature distribution

$$\frac{\partial\theta}{\partial\theta}\left(r = 1, \theta, \frac{a'}{b'} = 0\right) = -\frac{3}{2+k}\sin\theta. \tag{37}$$

In figure 7, Φ is plotted as a function of a'/b' for different values of k.

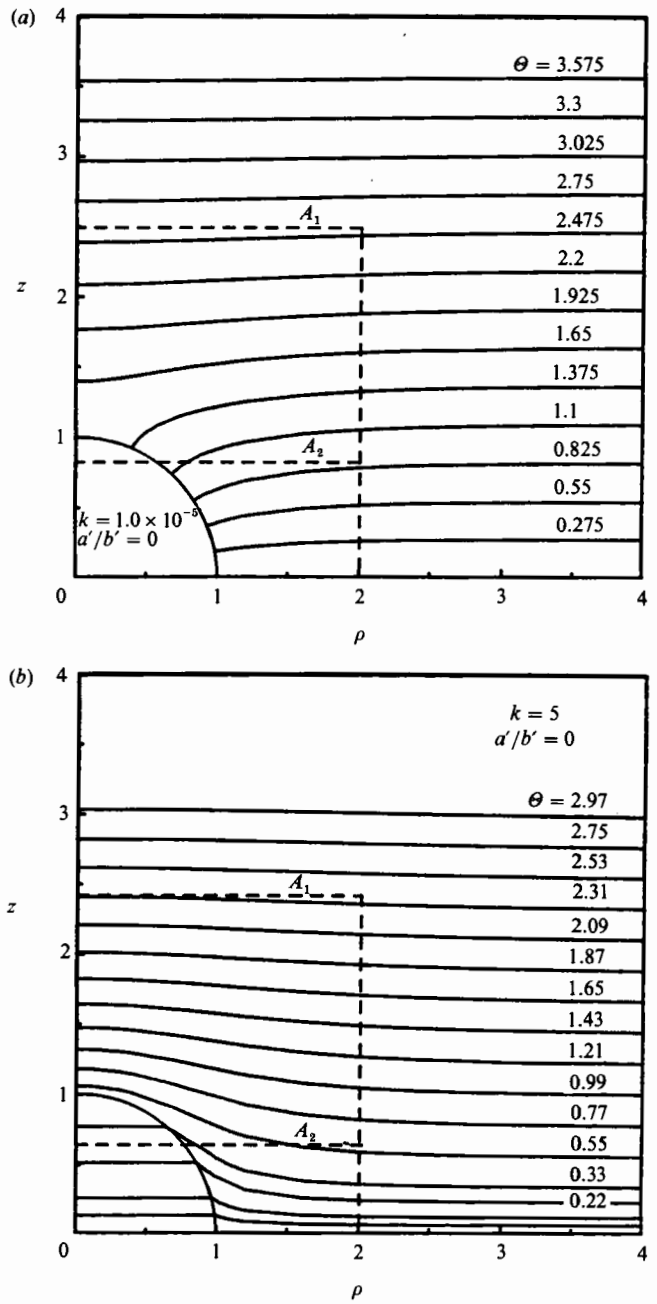

FIGURE 2. Contour plot of the non-dimensional temperature isotherms ($\Theta(z,\rho) = C$) for an infinite continuous phase subject to a far-field temperature gradient in the z-direction. The non-dimensional temperatures along the isotherms differ by a constant amount denoted by $\Delta\Theta$. (*a*) Isotherms around a gas bubble ($k = 1.0 \times 10^{-5}$), $\Delta\Theta = 0.275$ and (*b*) isotherms for a highly conducting liquid drop ($k = 5$), $\Delta\Theta = 0.22$.

Physical interpretation and discussion of the temperature results as given in figures 2–7 begins with the examination of the influence of the thermal conductivity ratio k. For the infinite system, if the conductivity ratio becomes just less than one, there is less resistance to conduction in the continuous phase, and a greater

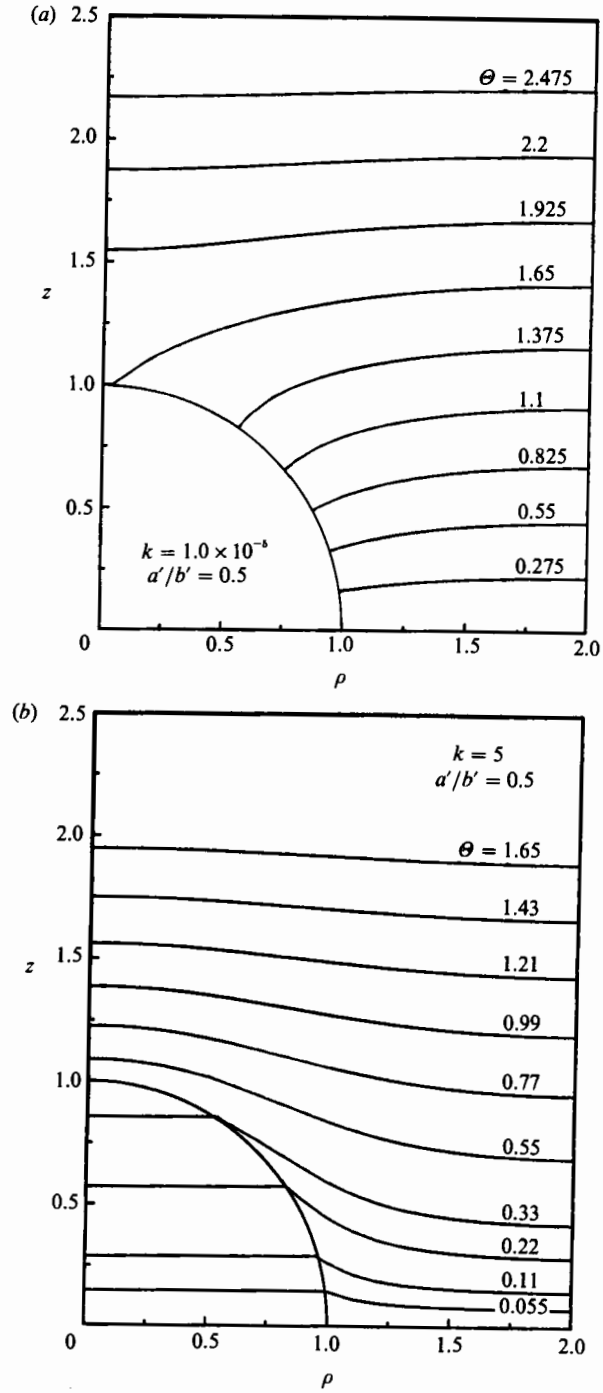

FIGURE 3. Isotherm contour plot for a fluid particle to tube radius, a'/b', equal to 0.5. (*a*) Isotherms around a gas bubble ($k = 1.0 \times 10^{-5}$), $\Delta\Theta = 0.275$ and (*b*) isotherms for a highly conducting liquid drop ($k = 5$), $\Delta\Theta = 0.22$.

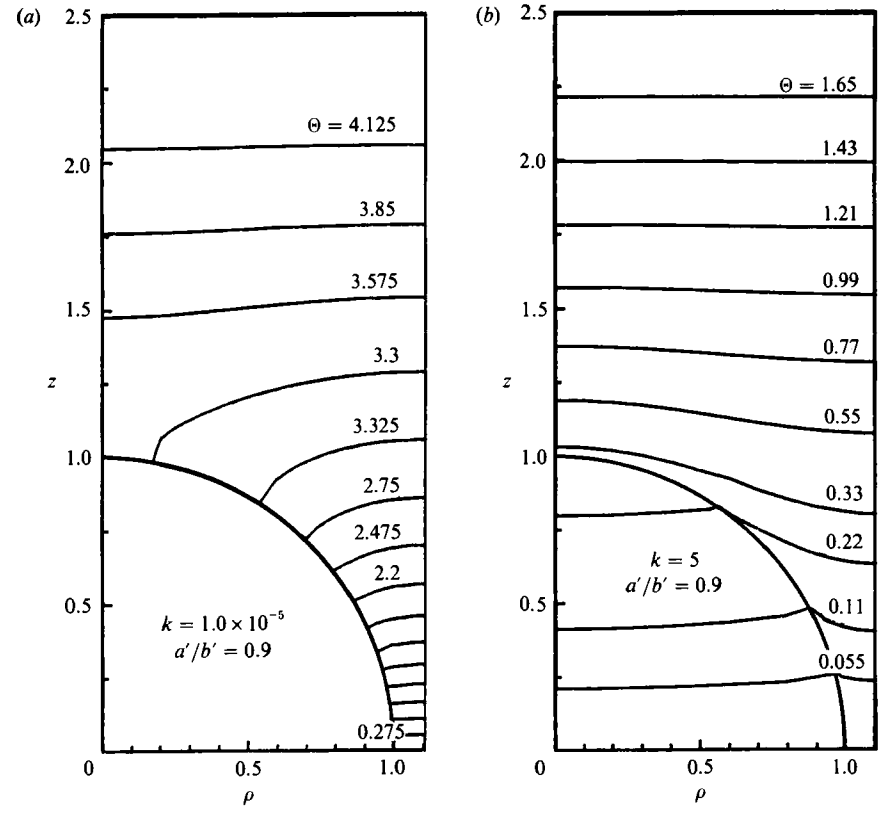

FIGURE 4. Isotherm contour plot for a fluid particle to tube radius, a'/b', equal to 0.9. (*a*) Isotherms around a gas bubble ($k = 1.0 \times 10^{-5}$), $\Delta\Theta = 0.275$ and (*b*) isotherms for a highly conducting liquid drop ($k = 5$), $\Delta\Theta = 0.22$.

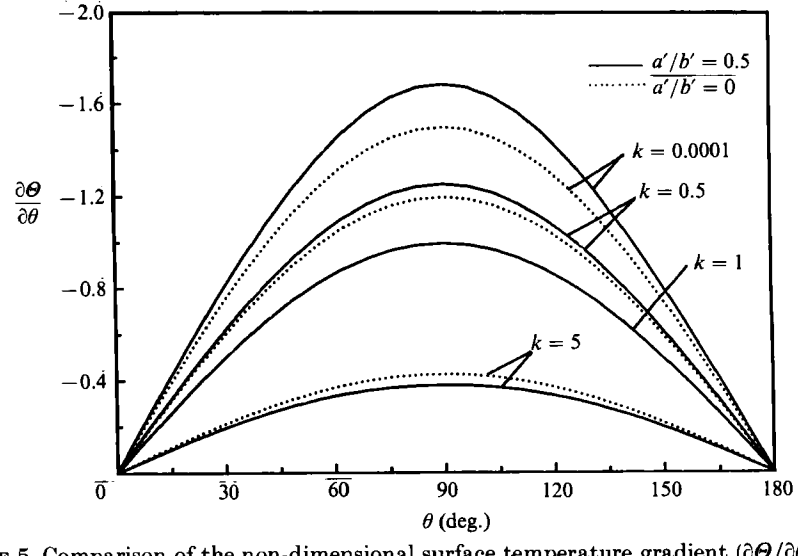

FIGURE 5. Comparison of the non-dimensional surface temperature gradient $(\partial\Theta/\partial\theta)(r = 1, \theta)$ as a function of θ for different values of the conductivity ratio k, and for a fluid particle to tube diameter ratio, a'/b', equal to 0.5. Plotted alongside (the dotted lines) are the surface gradient for an infinite system and the same values of k.

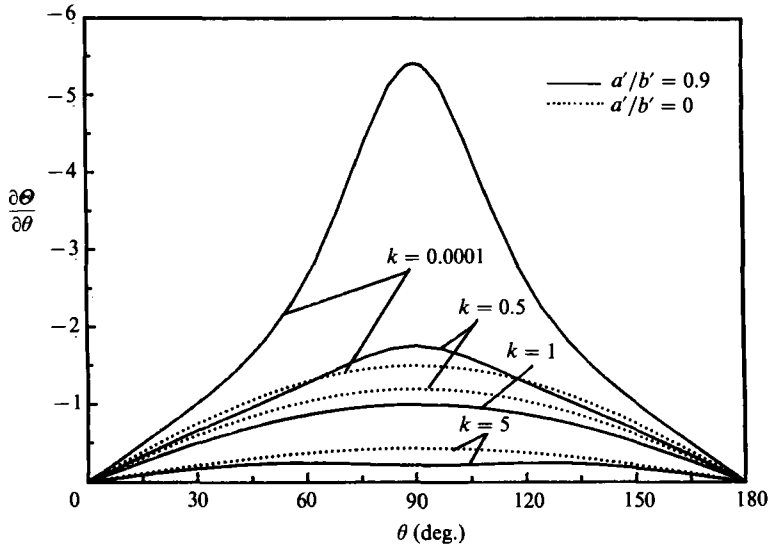

FIGURE 6. Comparison of the non-dimensional surface temperature gradient as a function of θ for different values of the conductivity ratio k, and for a fluid particle to tube diameter ratio, a'/b', equal to 0.9. Plotted alongside (the dotted lines) are the surface gradient for an infinite system and the same values of k.

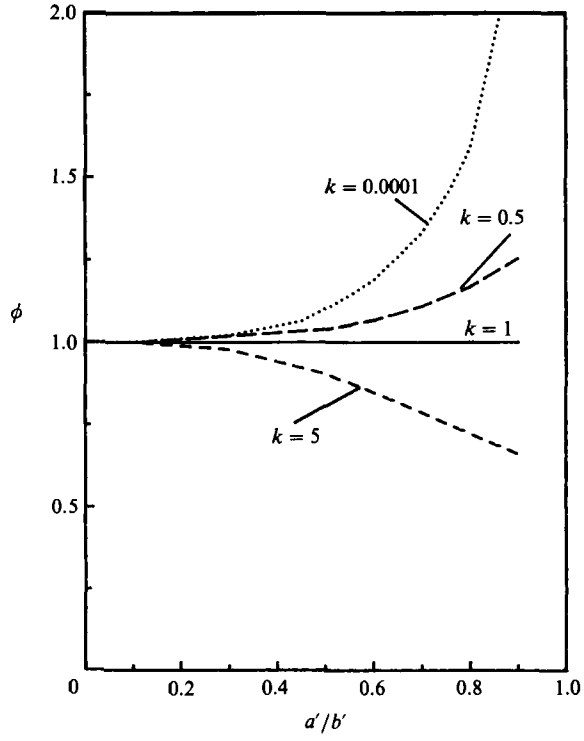

FIGURE 7. Plot of Φ, the quotient of the difference in the pole temperatures $\Theta(r = 1, 0) - \Theta(r = 1, \pi)$, for a fluid particle in a tube divided by that difference for a fluid particle in an infinite medium as a function of a'/b' for different values of k.

proportion of the energy is conducted through the suspending phase. As a consequence of this heat flow pattern, the temperature isotherms beginning at $\rho \to \infty$ and perpendicular to the z-axis bend towards the sphere (figure 2a). Therefore, relative to the case of $k = 1$ which represents a linear temperature field, the temperature difference between the poles and the temperature gradient along the sphere surface is increased (cf. the dotted lines in figures 5 and 6). As k decreases further from one, the temperature gradient and difference in pole temperatures continues to increase, as more heat is transported around the sphere. In the limit in which the conductivity of the sphere becomes equal to zero, all energy is conducted around the sphere and the isotherms intersect the fluid particle surface at right angles. The behaviour is reversed when k becomes just larger than one. A greater proportion of the energy is now transported through the sphere. The temperature isotherms starting at infinity bend away from the sphere (figure 2b) and the pole temperature difference and surface temperature gradient are decreased relative to $k = 1$ (figures 5 and 6). As k increases further from one, the temperature difference between the poles decreases, and the gradient along the surface is uniformly reduced. In the limit in which the sphere becomes infinitely conducting, the sphere surface becomes an isotherm and only the equatorial plane isotherm intersects the sphere surface. In this case, as is evident from (37), the temperature gradient becomes equal to zero.

In the confined geometry (figures 3 and 4), the effect of the conductivity ratio is similar to the behaviour explained above for an infinite expanse of a continuous phase. As is evident from figures 3(a) and 4(a) for a non-conducting sphere ($k = 1.0 \times 10^{-5}$), isotherms (now originating at the tube wall and perpendicular to it) bend towards the sphere to allow the heat to be transported through the more conductive continuous phase. Again as k decreases from one, the temperature gradient along the surface increases relative to the $k = 1$ distribution, and this is clearly shown in figures 5 and 6 for $a'/b' = 0.5$ and 0.9, respectively. The more important point is how this increase in surface gradient compares with that realized for the infinite case. Figures 5 and 6 indicate that as k decreases, the temperature gradient for the confined geometry increases more rapidly than the gradient for the infinite case. Thus for any particular value of $k < 1$, the surface temperature gradient is larger for the fluid particle in the tube than in an infinite amount of fluid. This central conclusion can be shown more clearly in terms of the Φ, the quotient in pole temperature differences. As detailed in figure 7, Φ increases as k decreases from one.

The reason why, for k less than one, the surface temperature gradient is larger in the tube than in an infinite medium can be understood very simply. Consider the isotherms for the infinite system figure 2(a), and superimpose onto this isotherm plot, a conceptual volume consisting of a tube of radius b' ($> a'$) closed at both ends and placed with its centreline coincident with the z-axis of the infinite system coordinates. The ends of the tube are located at a sufficiently large distance from the sphere so that at these ends the temperature gradient is unperturbed by the sphere and is therefore in the z-direction with magnitude $(\nabla' T')_\infty$. For $z > 0$, the surface which closes the tube is denoted by A_1. The amount of energy entering through A_1 is equal to $k^{(2)}(\nabla' T')_\infty \pi b'^2$. As figure 2($a$) indicates for $k < 1$, since the energy is transported around the sphere, there is a net flux of energy out of the inscribed boundary for the region above the equatorial plane. For the case of conduction in a tube, since the cylindrical portion of the tube boundary is insulated, no such heat loss occurs, yet the heat entering the tube is again $k^{(2)}(\nabla' T')_\infty \pi b'^2$. Consequently, for any cross-sectional area A_2 above the equatorial plane, the energy conducted through A_2 must be larger

in the tube than in the infinite geometry, and therefore the area averaged temperature gradient in the z-direction must be larger in the case of the tube. This increase in the z-component of the temperature gradient in the tube relative to that in an infinite medium accounts for the relative increase in the temperature gradient on the fluid particle surface.

For the opposite case of $k > 1$, the isotherms of the finite system originating from and perpendicular to the tube wall bend away from the sphere (figures 3*b* and 4*b*) so that a greater proportion of energy is conducted through the less resistive sphere. As k increases from one, the temperature gradient along the surface decreases and this is shown in figures 5 and 6. This behaviour of course is qualitatively the same as that of the infinite system as described above. However, figures 5 and 6 show that for $k > 1$, the temperature gradient in the tube is reduced more than it is in the infinite system as k increases. This marked reduction, as k increases from one, in the Marangoni driving force compared to that realized in the infinite system is clearly evident in the graph of Φ, figure 7.

The reason why, for $k > 1$, the temperature gradients along the surface of the sphere are less in the tube than in the infinite system can again be understood using control volume arguments. Specifically, consider the tube of radius b' superimposed on the isotherm contour diagram for the infinite system for $k > 1$ (figure 2*b*). The enclosing top surface of the tube is again denoted by A_1 and a representative cross-sectional area above the equator is identified by A_2. Energy is now conducted into the superimposed tube region for the infinite system case since the isotherms bend away from the sphere enabling more energy to pass through the sphere. Therefore the energy flux through A_2 must be larger in the infinite case than in the tube case because no energy can pass through the tube wall in the tube case. The temperature gradient in the z-direction is correspondingly greater, and this explains why the temperature gradient along the surface is larger in the infinite case.

The last result to comment upon is the dependence of the isotherm contours and the surface temperature gradients on the sphere to tube diameter ratio. For k fixed and less than one, as b'/a' decreases, the isotherm contours of figures 2(*a*), 3(*a*), and 4(*a*) establish that the temperature gradient along the surface increases. When $k > 1$, the opposite behaviour is obtained. These results follow for the same reasons that for $k < 1$ the surface temperature gradient is larger in the tube than in an infinite system, while for $k > 1$ the gradient is smaller.

To summarize the results for the temperature gradient along the surface: when $k < 1$, energy is conducted around the sphere. The surface gradient for a fluid particle in a tube is larger than the gradient on the surface of a fluid particle in an infinite medium, and this difference increases as b'/a' decreases. For $k > 1$, a greater proportion of the energy is transported through the particle. The surface gradient on the fluid particle surface is less than the gradient developed when the fluid particle is in an infinite medium, and the absolute value of this difference increases as b'/a' decreases.

3.2. *Hydrodynamic forces*

The hydrodynamic force in the z-direction (F'_z) exerted by the exterior fluid on the drop or bubble is obtained by integrating the viscous traction and pressure forces over the fluid particle surface. The force may be expressed in the following form (Happel & Brenner 1973):

$$F'_z = 4\pi a' \mu'^{(2)} U'_0 F_2^{(2)}, \tag{38}$$

where the constant $F_2^{(2)}$ is obtained as part of the solution of the system of equations as given in (35). As outlined in the previous section, the flow and therefore the

a'/b'	λ_u	Haberman & Sayre λ_u	Wang & Skalak λ_u
0.0	1.000	1.000	1.000
0.1	1.2632	1.263	1.263
0.2	1.6795	1.680	1.680
0.3	2.370	2.371	2.370
0.4	3.591	3.596	3.592
0.5	5.94	5.970	5.949
0.6	11.09	11.135	11.10
0.7	24.665	24.955	24.70
0.8	74.567	73.555	74.97
0.9	464.97		

TABLE 2. Comparison of converged values of drag coefficients λ_u with the results of Haberman & Sayre (1958) and Wang & Skalak (1969) for a solid particle ($\kappa = 10^8$)

hydrodynamic forces exerted on the fluid particle may be considered to be composed of the sum from two flow idealizations, one in which the temperature gradient is equal to zero, and the wall is moving creating a flow which drags against the particle, and a second idealization in which the wall is stationary and a Marangoni stress gives rise to fluid motion and a resulting lift force. The forces from each of these flow idealizations are discussed separately below.

Consider first the drag exerted on the fluid particle by the exterior flow caused by the movement of the wall only. This idealization is described by (35) with the temperature gradient set equal to zero, and the dimensional drag is given by

$$F'_{zu} = 4\pi a' \mu'^{(2)} U'_0 F^{(2)}_{2U} U. \tag{39}$$

The constant $F^{(2)}_{2U}$ is obtained by the collocation procedure and is tabulated in terms of a drag coefficient λ_u which is defined as the ratio of the drag on the fluid particle in this idealization to the drag exerted by the fluid particle in an infinite medium with uniform flow of the same magnitude, U'. This latter drag is equal to $-4\pi a' U' \mu'^{(2)}(1+\frac{3}{2}\kappa)/(1+\kappa)$ (cf. for example, Happel & Brenner 1973) and therefore the drag coefficient is defined by:

$$\lambda_u = \frac{-F^{(2)}_{2U}(1+\kappa)}{(1+\frac{3}{2}\kappa)}. \tag{40}$$

In the second problem, the wall is stationary and the Marangoni force causes fluid streaming and an associated lift force. This idealization is described by (35) with $U = 0$, and the drag is given by:

$$\begin{aligned} F'_{zm} &= 4\pi a' \mu'^{(2)} U'_0 F^{(2)}_{2M} \\ &= 4\pi a'^2 F^{(2)}_{2M} \left(-\frac{\partial \sigma'}{\partial T'}\right) (\nabla' T')_\infty / ((1+\tfrac{3}{2}\kappa)(2+k)). \end{aligned} \tag{41}$$

The lift coefficient λ_m is defined as the ratio of this force F'_{zm} exerted on the sphere in the tube divided by the lift force exerted on the sphere in an infinite, stationary, medium owing to the fluid streaming arising from a Marangoni force derived from an equal temperature gradient. The force in the infinite medium is equal to $4\pi a'^2(-\partial\sigma'/\partial T')(\nabla' T')_\infty/((1+\kappa)(2+k))$. (Note that this lift force is balanced by the drag, $-4\pi a' U'_0 \mu'^{(2)}(1+\frac{3}{2}\kappa)/(1+\kappa)$, which is due to the forward motion of the particle,

a'/b'	κ	λ_u	Hyman & Skalak λ_u
0.1	0	1.1632	1.16
	0.5	1.1947	
	1.0	1.2111	1.211
	2.0	1.228	
0.2	0	1.3899	1.390
	0.5	1.4745	
	1.0	1.5209	1.520
	2.0	1.5703	
0.3	0	1.7251	1.725
	0.5	1.8957	
	1.0	1.9951	1.995
	2.0	2.1059	
0.4	0	2.2626	2.263
	0.5	2.5714	
	1.0	2.7646	2.765
	2.0	2.992	
0.5	0	3.2223	3.222
	0.5	3.7559	
	1.0	4.1195	4.123
	2.0	4.5767	
0.6	0	5.2040	5.205
	0.5	6.1157	
	1.0	6.8064	6.808
	2.0	7.7475	
0.7	0	10.256	10.26
	0.5	11.832	
	1.0	13.216	13.22
	2.0	15.305	
0.8	0	28.553	28.59
	0.5	31.252	
	1.0	34.398	34.47
	2.0	39.864	
0.9	0	172.81	
	0.5	173.05	
	1.0	182.19	
	2.0	203.92	

TABLE 3. Comparison of converged values of drag coefficients λ_u with the results of Hyman & Skalak's solution (1970) for a fluid droplet

and (1) in fact follows easily by summing these forces to zero.) The lift coefficient λ_m, defined as the quotient of the actual Marangoni lift exerted in the tube divided by the lift in an infinite medium, is therefore given by:

$$\lambda_m = \frac{F^{(2)}_{2M}(1+\kappa)}{(1+\frac{3}{2}\kappa)}. \tag{42}$$

The calculations were checked by comparing values obtained for the drag coefficients to known values for certain limiting situations. Three verifications were done: first, the values for λ_u as a function of a'/b' for a solid sphere (implemented here by setting $\kappa = 10^8$) were compared with the results of Haberman & Sayre (1958) and Wang & Skalak (1969) assuming *a priori* solid spheres (i.e. using the no-slip condition). This comparison is given in table 2, and it can clearly be seen that the coefficients obtained in this study are within 1% of those from the past studies.

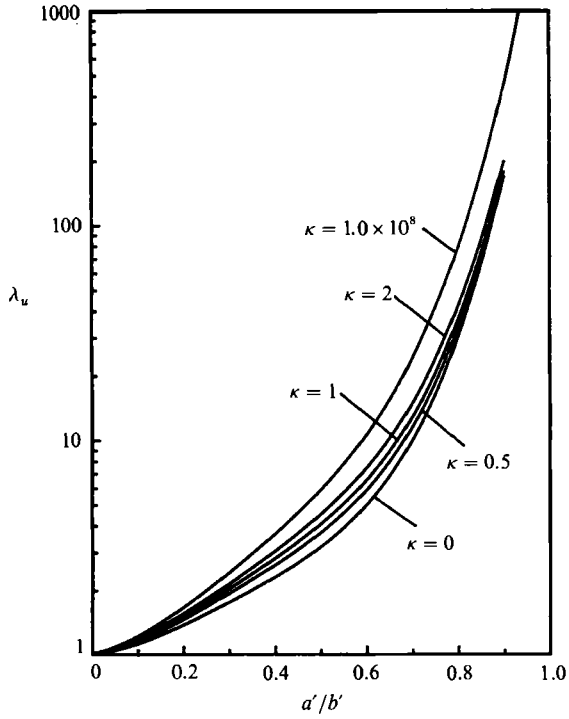

FIGURE 8. Graph of the drag coefficient λ_u for the movement of the tube wall past a fixed fluid particle as a function of the fluid particle to tube diameter ratio and for different values of the viscosity ratio, κ.

Additional verification of the λ_u calculations is obtained by comparing the results for a fluid sphere to those of Hyman & Skalak (1970) (table 3). This comparison is shown in table 3 for values of $\kappa = 0$ and 1 (the only two values studied by Hyman & Skalak); again the agreement is excellent. No previous studies have computed λ_m, and therefore the only way of checking these results is to verify that they properly converge towards one for all κ and k as $a'/b' \to 0$. This behaviour will be evident in the graphs to be presented below.

Converged values for λ_u are plotted in figure 8, for respectively $\kappa = 0$, 0.5, 1.0, 2.0, and 10^8 (solid sphere) and for a range of a'/b' between 0 and 0.9. Figure 8 shows several interesting features. The figure indicates that λ_u increases as a'/b' increases for fixed κ. The dimensional drag (F'_{zu}) in terms of this drag coefficient is equal to $-4\pi a' \mu'^{(2)}((1+\frac{3}{2}\kappa)/(1+\kappa))\,\lambda_u U'$ and it represents the force exerted on a fixed sphere with the wall moving with a velocity U'. It can be concluded from figure 8 and the expression for F'_{zu} that for fixed viscosities and sphere diameter, the drag increases as the tube radius decreases. This increase in drag is due to the hydrodynamic interaction of the sphere with the wall: as the gap between the sphere perimeter and the tube wall decreases, the shear rate in the gap in the vicinity of the sphere increases. The sphere suffers a higher shear stress applied by the fluid, therefore the drag consequently increases. Also evident from figure 8 is the fact that the drag coefficient increases with κ at fixed a'/b'. As a physical example, increasing κ can be realized by varying the droplet viscosity with the continuous phase viscosity and the tube and fluid particle diameters held constant. For that case, the dimensional drag also increases since the factor $(1+\frac{3}{2}\kappa)/(1+\kappa)$ monotonically increases with κ along

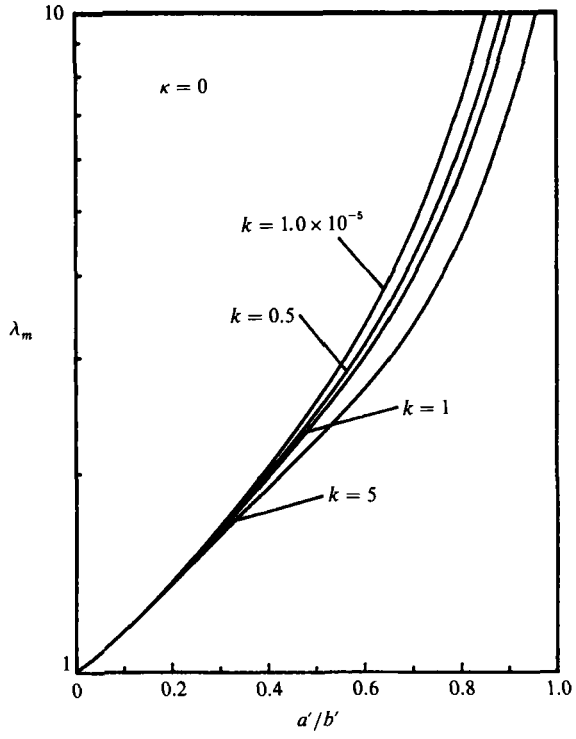

FIGURE 9. Lift force coefficient λ_m for the Marangoni driven streaming motion of the continuous phase past a fixed sphere and a stationary wall as a function of a'/b' and for different values of the conductivity ratio k. The figure is for a viscosity ratio, κ, equal to zero.

with λ_u. The reason for the increase in dimensional drag is also clear; as the droplet viscosity increases, the sphere surface velocity decreases and this causes the shear rate in the vicinity of the sphere to increase, thereby increasing the drag coefficient.

The converged results for λ_m as a function of a'/b' are detailed in figure 9 for different values of the conductivity ratio k and $\kappa = 0$, and in figure 10 for different values of the viscosity ratio κ and $k = 1.0 \times 10^{-5}$. Consider first the dependence on k, figure 9, and note the behaviour for $k = 1$. For equal thermal conductivities, figure 9 indicates that λ_m is larger than one, and increases with a'/b'. Recall that when $k = 1$, the surface temperature gradient is identical to that for the infinite case, and is therefore independent of a'/b'. Thus the fact that the lift forces in the tube case become increasingly larger than those in the infinite case cannot be due to an increase in the surface Marangoni force. The reason for this behaviour may be attributed to the pressure differential which develops across the sphere. In the flow idealization which defines λ_m, the surface force drives, in the continuous phase, a streaming flow in the vicinity of the fluid particle interface in the negative z-direction. Since the wall is stationary, and the fluid at infinity is at rest, the net flow rate for this streaming flow in the z-direction must be equal to zero. Therefore downstream from the particle, pressure forces develop to turn the fluid around. As this pressure force acts in the positive z-direction it provides, along with the reaction to the surface Marangoni force, the lift which propels the droplet in the positive z-direction. As the tube diameter decreases, for a constant Marangoni force, the surface velocity and therefore the magnitude of the streaming flow decreases. However, the pressure force which drives the recirculation does not decrease because it must drive fluid through

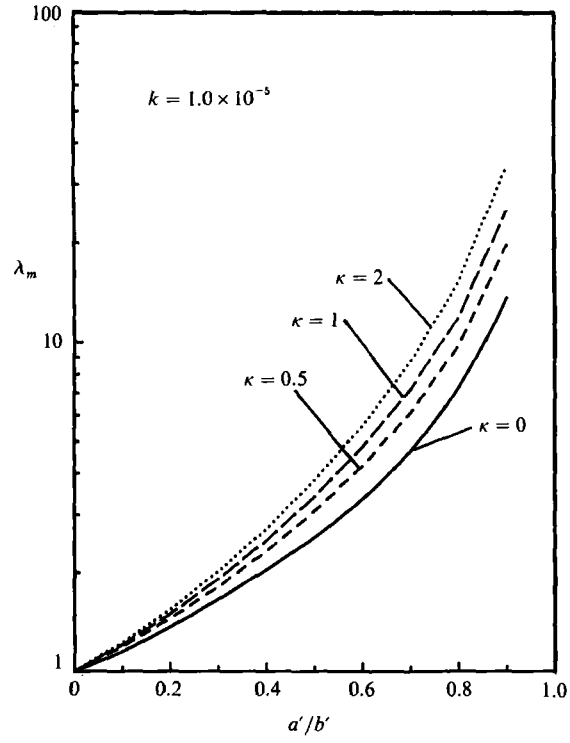

FIGURE 10. Lift force coefficient λ_m as a function of a'/b' for different values of the viscosity ratio, κ, and $k = 1.0 \times 10^{-5}$.

an increasingly smaller gap between the fluid particle and the tube surface. This fact is over-riding, and causes the pressure to increase as the tube diameter decreases. This increase in pressure manifests itself as an increase in the lift force, and explains why λ_m is larger than one for $k = 1$, and increases with a'/b'.

Consider next the dependence of λ_m on the conductivity ratio k. Figure 9 shows that as k decreases from one, λ_m increases and as k increases from one, λ_m decreases. This effect can be understood completely in terms of the influence of k (at fixed a'/b') on the surface temperature gradient as discussed in §3.1 (cf. figures 5–7): as k decreases from one, the surface temperature gradient in the tube geometry becomes increasingly larger than that which develops on a fluid particle in an infinite medium, and therefore λ_m, which is the ratio of the lift forces in the tube and infinite geometries, increases. Similarly, as k increases from one, the surface temperature gradient for the fluid particle in a tube decreases relative to the infinite medium value, and λ_m decreases. Note finally that since the dimensional lift force, F'_{zm}, is equal to $-4\pi a'^2(\partial\sigma/\partial T)(\nabla' T')_\infty \lambda_m/((1+\kappa)(2+k))$, for fixed fluid viscosities and sphere and tube diameters, the dimensional lift force increases as k decreases.

Consider next the dependence of λ_m on a'/b' for k not equal to one. Figure 9 shows that for all k, λ_m increases with a'/b'. Significantly, this increase is enhanced as k decreases. Reasons for this behaviour may be attributed to two effects, the back pressure which develops to recirculate the fluid and which increases with a'/b', and the influence of a'/b' on the surface temperature gradient (figure 7). When $k < 1$, the surface temperature gradient increases as a'/b' increases. This causes larger Marangoni stresses which act to increase the lift force. In addition, the back pressure increases because the gap thickness decreases. Thus λ_m should increase rapidly. For

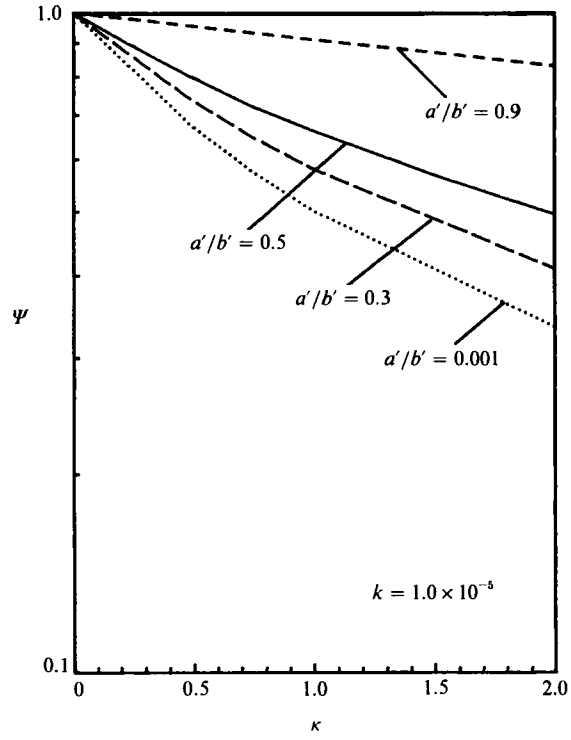

FIGURE 11. Graph of the ratio (Ψ) of the lift force F'_{zm} for a particular value of κ divided by that force for $\kappa = 0$ as a function of a'/b' and $k = 1.0 \times 10^{-5}$.

$k < 1$, these two influences have opposite effects. Although the back pressure increases with a'/b', the surface Marangoni force decreases (figure 7). However, as was the case with $k = 1$, the effect of the decreasing gap size on the back pressure is dominant, and λ_m slowly increases with a'/b'.

The dependence of λ_m on the fluid viscosity ratio κ is given in figure 10, and this figure indicates that for a fixed a'/b', λ_m increases with κ. To understand this dependence, consider first how the dimensional lift force behaves with κ for a fixed continuous phase viscosity and fluid particle radius a'. The dimensional lift (F'_{zm}), is plotted in figure 11, as a function of κ, for $k = 1.0 \times 10^{-5}$ as a function of κ, divided by the lift for the same a'/b' and $\kappa = 0$. This quotient, which is equal to $\lambda_m(\kappa, k = 1.0 \times 10^{-5}, a'/b')/\lambda_m(\kappa = 0, k = 10 \times 10^{-5}, a'/b')$ is defined as Ψ. Figure 11 indicates that as κ increases, Ψ and consequently the dimensional lift decreases. As κ increases, the velocity on the surface owing to the Marangoni force (which is independent of κ) decreases, and this causes the lift force to decrease. Reconsider figure 10: mathematically, the reason why λ_m increases with κ at fixed a'/b' is that, as is evident in figure 11 (for $k = 1.0 \times 10^{-5}$), the dimensional lift in the tube does not decrease as fast with κ as that for an infinite medium (the latter varies as $(1+\kappa)^{-1}$, and corresponds to the curve labelled $a'/b' = 10^{-3}$ in figure 11). Physically, this behaviour reflects the fact that in the infinite medium at finite κ, the droplet stress which retards the surface force is a larger percentage of the total retarding force (outside and inside) than it is in the confined geometry. The reason for this is that the lengthscale for the relaxation in the velocity in the unbounded geometry is much larger than in the confined one. When the interior viscosity is increased, the droplet stress is increased, and to maintain a constant surface force, a reduction in the

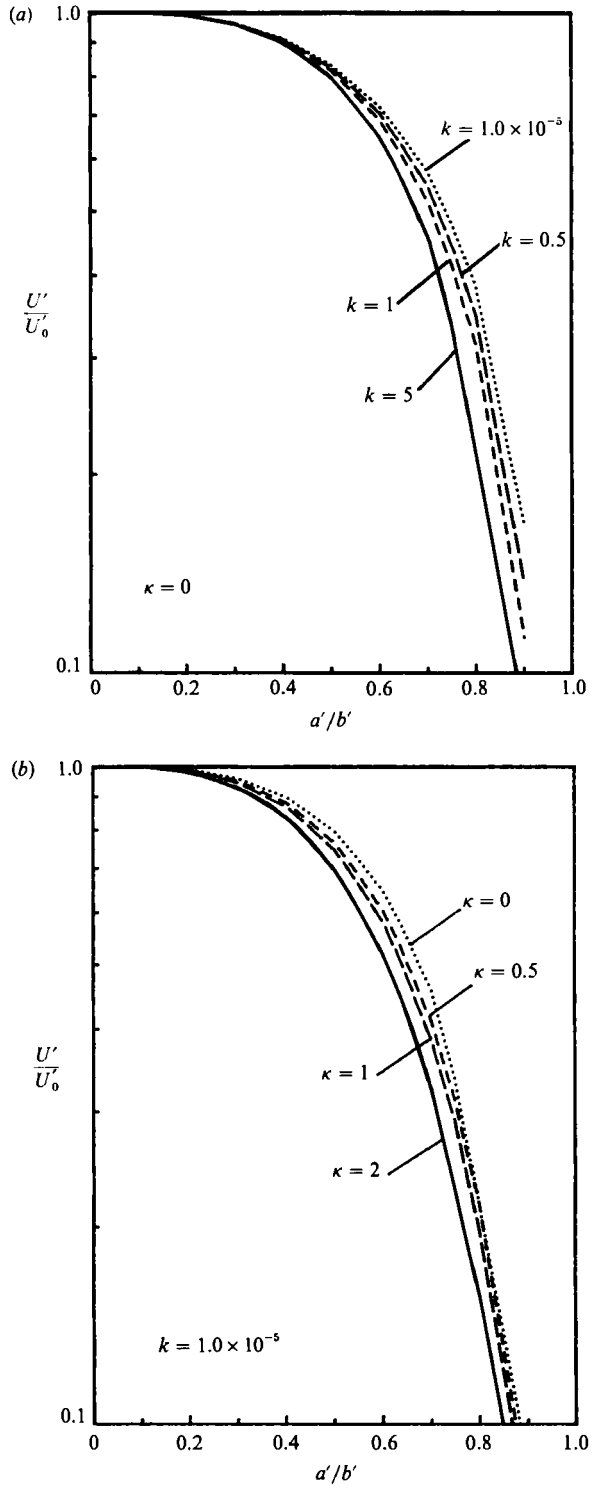

FIGURE 12. The ratio of the migration velocity in a tube to that in an infinite medium, U'/U_0', as a function of a'/b' for (*a*) $\kappa = 0$ and different values of k and (*b*) $k = 1.0 \times 10^{-5}$ and different values of κ.

surface velocity (relative to its previous value) is necessary. This reduction is larger in the unbounded than in the bounded case since the droplet stress is a larger component of the total retarding shear stress. Thus the proportional change in the drag is more for the unbounded case, and λ_m increases with κ.

3.3. *Terminal velocities*

The total force on the fluid particle ($F'_{zu}+F'_{zm}$) is equal to zero. This requirement allows the fluid particle velocity U' to be computed; using (39)–(42), U' may be expressed relative to the speed in an infinite medium (U'_0) through the drag and lift coefficients λ_u and λ_m:

$$\frac{U'}{U'_0} = \frac{\lambda_m}{\lambda_u}. \tag{43}$$

This equation clearly illustrates the competing effects which determine the relative speed: The enhancement of the Marangoni lift force relative to the infinite value, λ_m (figures 9 and 10), acts to increase the relative speed, while the enlargement (relative to the infinite system) of the drag force owing to the forward motion, λ_u (figure 8), retards the relative speed. The result of these competing effects is shown in figures 12(*a*) and 12(*b*) which graph U'/U'_0 as a function of a'/b' for different values of k (figure 12*a*) and κ (figure 12*b*). The principal observation from these graphs is that U'/U'_0 is always less than one, and is a monotonically decreasing function of a'/b' for all values of the conductivity and viscosity ratios. Hence, with increasing a'/b', the increased drag due to the hydrodynamic interaction of the fluid particle with the tube wall dominates the increase in the Marangoni lift force, and the fluid particle in the tube always moves slower than it does in an infinite medium. At a fixed ratio of the diameter of the fluid particle to that of the tube, the dependence of U'/U'_0 on k and κ follows directly from the dependencies of λ_m and λ_u on these variables. Consider first the behaviour with k: the drag coefficient λ_u is independent of k. The Marangoni lift coefficient, λ_m, increases with decreasing k as a greater proportion of the energy from infinity circumvents the fluid particle and creates a high surface-temperature gradient allowing the energy to pass through the narrow gap. Therefore, as indicated in figure 10, the relative speed increases with decreasing k. The dependence of U'/U'_0 on κ at fixed a'/b' is more complicated. In this case, although both λ_m and λ_u increase with κ, comparison of figures 8 and 10 indicate that the effect of the viscosity ratio on λ_u is greater than that on λ_m. Hence, as demonstrated in figure 12(*b*), the relative velocity decreases as the viscosity of the fluid particle becomes larger than that of the continuous phase.

4. Conclusions

This paper has examined the steady, creeping, thermocapillary migration of a spherical fluid particle in a tube owing to an imposed axial temperature gradient under conditions of axisymmetry, negligible thermal convection and an insulated tube wall. As outlined in §1, the intention of this study is to use this flow geometry as a model for understanding the influence of lateral wall–fluid particle hydrodynamic and thermal interactions in determining the thermocapillary migration velocity.

In this Stokes problem, the force of the continuous phase on the fluid particle can be divided into the forces from two fixed-fluid particle flow idealizations, one in which the tube wall is moving dragging fluid over the stationary fluid particle with no Marangoni force, and a second idealization in which the wall is fixed and the

surface temperature gradient drives a streaming, recirculating motion that propels the fluid particle towards the warmer fluid. The dragging force is described by a drag coefficient λ_u, and the thermocapillary lift or propulsion force is described by a lift coefficient λ_m. Each of these coefficients represents the ratio of the force in the idealization in the confined tube geometry divided by that in an infinite medium. The first idealization and the coefficient λ_u describe the hydrodynamic resistance of the wall on the forward motion of the particle. This coefficient increases sharply as the sphere to tube diameter ratio increases. The second idealization and the lift coefficient λ_m describe the thermal interaction between the wall and the particle. The lift coefficient increases as the ratio of the fluid particle to the continuous phase liquid conductivity decreases since in that limit more energy is conducted through the gap between the fluid particle and the wall, and this heat flow intensifies the fluid particle surface temperature gradient. This increase is enhanced as the gap thickness decreases. The lift coefficient also describes a secondary wall–fluid particle hydrodynamic interaction apart from the resistance to forward motion as described by λ_u. Specifically, for the case in which the conductivities of the fluid particle and the continuous phase are equal, and therefore the thermal interaction is equal to zero, the lift coefficient λ_m increases as the gap distance between the fluid particle and the wall decreases. The increase is ascribed to the increase in the back pressure which drives the recirculating motion of the Marangoni flow idealization, and which propels the fluid particle towards the warmer temperature. This back pressure increases with decreasing gap thickness because a higher back pressure is necessary to drive fluid through a narrowing gap.

The ratio of λ_m to λ_u determines the migration velocity in the tube relative to that in an infinite medium. Calculations of this ratio indicate that, for a fixed gap thickness, the relative velocity increases as the fluid particle conductivity decreases, and that this increase in migration becomes more pronounced as the gap thickness decreases. Both these results are attributable to the influence of the thermal interaction on λ_m. However, for a fixed, small conductivity ratio, the relative velocity decreases as the gap thickness decreases, and this reflects the predominance of the hydrodynamic retardation of the wall on the forward motion (as described by λ_u) over the migration enhancing thermal interaction and secondary back pressure hydrodynamic interaction (as given by λ_m).

This work was supported in part by a grant from the Department of Energy, Office of Basic Energy Sciences (DE-FG02-88ER13820), to C.M. and a grant from the National Science Foundation to Z.D.

Appendix

Expressions for the G_n^k functions are given below.

$$G_n^1(\rho,z) = (\rho^2+z^2)^{-\frac{1}{2}(n+1)} P_n\left[\frac{z}{(\rho^2+z^2)^{\frac{1}{2}}}\right],$$

$$G_n^2(\rho,z) = (\rho^2+z^2)^{-\frac{1}{2}(n-1)}\left[P_n\left[\frac{z}{(\rho^2+z^2)^{\frac{1}{2}}}\right]+2C_n^{-\frac{1}{2}}\left[\frac{z}{(\rho^2+z^2)^{\frac{1}{2}}}\right]\right],$$

$$G_n^3(\rho,z) = (\rho^2+z^2)^{-\frac{1}{2}(n-1)} C_n^{-\frac{1}{2}}\left[\frac{z}{(\rho^2+z^2)^{\frac{1}{2}}}\right],$$

$$G_n^4(\rho,z) = (\rho^2+z^2)^{-\frac{1}{2}(n-3)} C_n^{-\frac{1}{2}}\left[\frac{z}{(\rho^2+z^2)^{\frac{1}{2}}}\right],$$

$$G_n^5(\rho,z) = \frac{(n+1)}{\rho}(\rho^2+z^2)^{-\frac{1}{2}n} C_{n+1}^{-\frac{1}{2}}\left[\frac{z}{(\rho^2+z^2)^{\frac{1}{2}}}\right],$$

$$G_n^6(\rho,z) = \frac{(n+1)}{\rho}(\rho^2+z^2)^{-\frac{1}{2}(n-2)} C_{n+1}^{-\frac{1}{2}}\left[\frac{z}{(\rho^2+z^2)^{\frac{1}{2}}}\right] - \frac{2z}{\rho}(\rho^2+z^2)^{-\frac{1}{2}(n-1)} C_n^{-\frac{1}{2}}\left[\frac{z}{(\rho^2+z^2)^{\frac{1}{2}}}\right]. \tag{A 1}$$

Expressions for the terms H_n^i are:

$$\left.\begin{aligned}
H_n^1(t) &= (-1)^{\frac{1}{2}n}\frac{2}{\pi n!}t^n K_0(Rt),\\
H_n^2(t) &= -(-1)^{\frac{1}{2}n}\frac{2}{\pi n!}t^{n-2}[n(n-1)K_0(Rt) - (2n-3)RtK_1(Rt)],\\
H_n^3(t) &= -(-1)^{\frac{1}{2}n}\frac{2}{\pi n!}Rt^{n-1}K_1(Rt),\\
H_n^4(t) &= -(-1)^{\frac{1}{2}n}\frac{2}{\pi n!}Rt^{n-3}[(2n-3)RtK_0(Rt) - (n-2)(n-3)K_1(Rt)].
\end{aligned}\right\} \tag{A 2}$$

The functions S_n^q are defined as:

$$\left.\begin{aligned}
S_n^1(r,\theta) &= r^{-n+1}C_n^{-\frac{1}{2}}(\cos\theta) + \int_0^\infty \mathrm{d}t\cos(tr\cos\theta)[T_n^1(t)\,r\sin\theta I_1(tr\sin\theta)\\
&\quad + T_n^3(t)(r\sin\theta)^2 I_0(tr\sin\theta)],\\
S_n^2(r,\theta) &= r^{-n+3}C_n^{-\frac{1}{2}}(\cos\theta) + \int_0^\infty \mathrm{d}t\cos(tr\cos\theta)[T_n^2(t)\,r\sin\theta I_1(tr\sin\theta)\\
&\quad + T_n^4(t)(r\sin\theta)^2 I_0(tr\sin\theta)],\\
\begin{bmatrix}S_n^3\\ S_n^4\end{bmatrix} &= P_{n-1}(\cos\theta) + \int_0^\infty \mathrm{d}t\left\{t\sin\theta\sin(t\cos\theta)\left(\begin{bmatrix}T_n^1\\ T_n^2\end{bmatrix} I_1(t\sin\theta)\right.\right.\\
&\quad \left. + \begin{bmatrix}T_n^3\\ T_n^4\end{bmatrix}\sin\theta I_0(t\sin\theta)\right) + \cos\theta\cos(t\cos\theta)\left(\begin{bmatrix}T_n^1\\ T_n^2\end{bmatrix} tI_0(t\sin\theta)\right.\\
&\quad \left.\left. + \begin{bmatrix}T_n^3\\ T_n^4\end{bmatrix}(2I_0(t\sin\theta) + t\sin\theta I_1(t\sin\theta))\right)\right\},\\
\begin{bmatrix}S_n^5\\ S_n^6\end{bmatrix} &= \begin{bmatrix}(1-n)\\ (3-n)\end{bmatrix}\frac{C_n^{-\frac{1}{2}}(\cos\theta)}{\sin\theta} + \int_0^\infty \mathrm{d}t\left\{t\cos\theta\sin(t\cos\theta)\left(-\begin{bmatrix}T_n^1\\ T_n^2\end{bmatrix} I_1(t\sin\theta)\right.\right.\\
&\quad \left. - \begin{bmatrix}T_n^3\\ T_n^4\end{bmatrix}\sin\theta I_0(t\sin\theta)\right) + \sin\theta\cos(t\cos\theta)\left(\begin{bmatrix}T_n^1\\ T_n^2\end{bmatrix} tI_0(t\sin\theta)\right.\\
&\quad \left.\left. + \begin{bmatrix}T_n^3\\ T_n^4\end{bmatrix}(2I_0(t\sin\theta) + t\sin\theta I_1(t\sin\theta))\right)\right\},\\
\begin{bmatrix}S_n^7\\ S_n^8\end{bmatrix} &= \begin{bmatrix}S_n^5\\ S_n^6\end{bmatrix} - \begin{bmatrix}(n^2-1)\\ (3-n)(1-n)\end{bmatrix}\frac{C_n^{-\frac{1}{2}}(\cos\theta)}{\sin\theta}
\end{aligned}\right\}$$

$$
\left.
\begin{aligned}
&-\int_0^\infty \mathrm{d}t \Bigg\{ \cos(t\cos\theta) \left(\begin{bmatrix} T_n^1 \\ T_n^2 \end{bmatrix} t^2(\sin^2\theta - \cos^2\theta) I_1(t\sin\theta) \right. \\
&\left. + \begin{bmatrix} T_n^3 \\ T_n^4 \end{bmatrix} \sin\theta (t^2(\sin^2\theta - \cos^2\theta) I_0(t\sin\theta) + 2t\sin\theta I_1(t\sin\theta)) \right) \\
&- t\cos\theta \sin(t\cos\theta) \left(\begin{bmatrix} T_n^1 \\ T_n^2 \end{bmatrix} (2t\sin\theta I_0(t\sin\theta) - I_1(t\sin\theta)) \right. \\
&\left. + \begin{bmatrix} T_n^3 \\ T_n^4 \end{bmatrix} \sin\theta (3I_0(t\sin\theta) + 2t\sin\theta I_1(t\sin\theta)) \right) \Bigg\},
\end{aligned}
\right\} \tag{A 3}
$$

where the functions $T_n^i(t)\,(i = 1, 2, 3, 4)$ are defined as

$$
\left.
\begin{aligned}
T_n^1(t) &= [(2 + Rt\Omega) H_n^3(t) - R^2 H_n^1(t)]/\Delta, \\
T_n^2(t) &= [(2 + Rt\Omega) H_n^4(t) - R^2 H_n^2(t)]/\Delta, \\
T_n^3(t) &= [R\Omega H_n^1(t) - tH_n^3(t)]/\Delta, \\
T_n^4(t) &= [R\Omega H_n^2(t) - tH_n^4(t)]/\Delta.
\end{aligned}
\right\} \tag{A 4}
$$

The variable Ω is given by $I_1(Rt)/I_0(Rt)$ and

$$\Delta = R^2 t I_0(Rt) - 2RI_1(Rt) - R^2 t I_1(Rt)\,\Omega.$$

REFERENCES

Anderson, J. L. 1985 Droplet interactions in thermocapillary motion. *Intl J. Multiphase Flow* **11**, 813.

Annamalai, P., Shankar, R., Cole, R. & Subramanian, R. S. 1982 Bubble migration inside a liquid drop in a space laboratory. *Appl. Sci. Res.* **38**, 179.

Ascoli, E. P. & Leal, L. G. 1990 Thermocapillary motion of a deformable drop toward a planar wall. *J. Colloid Interface Sci.* **138**, 220.

Balasubramaniam, R. & Chai, A.-T. 1987 Thermocapillary migration of droplets: An exact solution for small Marangoni numbers. *J. Colloid Interface Sci.* **119**, 531.

Barton, D. & Subramanian, R. S. 1990 Thermocapillary migration of a liquid drop normal to a plane surface. *J. Colloid Interface Sci.* **137**, 170.

Bergman, A., Carlberg, T., Fredriksson, H. & Stjerndahl, J. 1982 The influence of gravity on the solidification of monotectic and near monotectic Cu–Pb alloys. In *Materials Processing in the Reduced Gravity Environment of Space* (ed. G. E. Rindone).

Bratukhin, Y. K. 1976 Thermocapillary drift of a viscous fluid droplet. *NASA Tech. Trans. NASA TT F* 17093.

Chen, S. H. & Keh, H. J. 1990 Thermocapillary motion of a fluid droplet normal to a plane surface. *J. Colloid Interface Sci.* **137**, 550.

Feuillebois, F. 1989 Thermocapillary migration of two equal bubbles parallel to their line of centers. *J. Colloid Interface Sci.* **131**, 267.

Haberman, W. L. & Sayre, R. M. 1958 Motion of rigid and fluid spheres in stationary and moving liquids inside cylindrical tubes. *David W. Taylor Model Basin Report* no. 1143, US Navy Dept.

Happel, H. & Brenner, H. 1973 *Low Reynolds Number Hydrodynamics*. Noordhoof.

Hariri, H. H., Nadim, A. & Borhan, A. 1990 Effect of inertia on the thermocapillary velocity of a drop. *J. Colloid Interface Sci.* **140**, 277.

Hasan, M. M. & Balasubramaniam, R. 1989 Thermocapillary migration of a large gas slug in a tube. *J. Thermophys.* **3**, 87.

HYMAN, W. A. & SHALAK, R. 1970 *Tech. Rep.* no. 5, Proj. no. NR 062-393, Dept. Civil Engng and Engng Mech., Columbia University.

KEH, H. J. & CHEN, S. H. 1990 The thermocapillary motion of two droplets along their line of centers. *Intl J. Multiphase Flow* **16**, 515.

KIM, H. S. & SUBRAMANIAN, R. S. 1989*a* Thermocapillary migration of a droplet with insoluble surfactant. *J. Colloid Interface Sci.* **127**, 417.

KIM, H. S. & SUBRAMANIAN, R. S. 1989*b* The thermocapillary migration of a droplet with insoluble surfactant. *J. Colloid Interface Sci.* **130**, 112.

LEICHTBERG, S., PFEFFER, R. & WEINBAUM, S. 1976 Stokes flow past finite coaxil clusters of spheres in a circular cylinder. *Intl J. Multiphase Flow* **3**, 147.

MARTINEZ, M. & UDELL, K. 1990 Axisymmetric creeping motion of drops through circular tubes. *J. Fluid Mech.* **210**, 565.

MEYYAPPAN, M. & SUBRAMANIAN, R. S. 1984 Thermocapillary motion of two bubbles oriented arbitrary relative to a thermal gradient. *J. Colloid Interface Sci.* **97**, 291.

MEYYAPPAN, M. & SUBRAMANIAN, R. S. 1987 Thermocapillary migration of a gas bubble in an arbitrary direction with respect to a plane surface. *J. Colloid Interface Sci.* **115**, 206.

MEYYAPPAN, M., WILCOX, W. R. & SUBRAMANIAN, R. S. 1981 Thermocapillary migration of a bubble normal to a plane surface. *J. Colloid Interface Sci.* **83**, 199.

MEYYAPPAN, M., WILCOX, W. R. & SUBRAMANIAN, R. S. 1983 The slow axisymmetric motion of two bubbles in a thermal gradient. *J. Colloid Interface Sci.* **94**, 243.

MORTON, D. S., SUBRAMANIAN, R. S. & BALASUBRAMANIAM, R. 1990 The migration of a compound drop due to thermocapillacity. *Phys. Fluids* **2**, 2119.

NADIM, A. & BORHAN, A. 1989 The effects of surfactants on the motion and deformation of a droplet in thermocapillary migration. *PhysicoChem. Hydrodyn.* **11**, 753.

SHANKAR, N., COLE, R. & SUBRAMANIAN, R. S. 1981 Thermocapillary migration of a fluid droplet inside a drop in a space laboratory. *Intl J. Multiphase Flow* **7**, 581.

SHANKAR, N. & SUBRAMANIAN, R. S. 1983 The slow axisymmetric thermocapillary migration of an eccentrically placed bubble inside a drop in zero gravity. *J. Colloid Interface Sci.* **94**, 258.

SHANKAR, N. & SUBRAMANIAN, R. S. 1988 The Stokes motion of a gas bubble due to interfacial tension gradients at low to moderate Marangoni numbers. *J. Colloid Interface Sci.* **123**, 512.

SUBRAMANIAN, R. S. 1981 Slow migration of a gas bubble in a thermal gradient. *AIChE J.* **27**, 646.

SUBRAMANIAN, R. S. 1983 Thermocapillary migration of bubbles and droplets. *Adv. Space Res.* **3** (5), 145.

THOMPSON, R. L., DEWITT, K. J. & LABUS, T. L. 1980 Marangoni bubble motion phenomenon in zero gravity. *Chem. Engng Commun.* **5**, 299.

WANG, H. & SHALAK, R. 1969 Viscous flow in a cylindrical tube containing a line of spherical particles. *J. Fluid Mech.* **38**, 75.

WEINBERG, M. C. 1978 Glass processing in space. *Glass Industry* **59**, 22.

YOUNG, N. O., GOLDSTEIN, J. S. & BLOCK, M. J. 1959 The motion of bubbles in a vertical temperature gradient. *J. Fluid Mech.* **6**, 350.